Enhanced Position Sensorless Control Using Bilinear Recursive Least Squares Adaptive Filter for Interior Permanent Magnet Synchronous Motor

Wu, Xuan; Huang, Sheng; Liu, Kan; Lu, Kaiyuan; Hu, Yashan; Pan, Wenli; Peng, Xiaoyuan

Published in:
IEEE Transactions on Power Electronics

DOI (link to publication from Publisher):
10.1109/TPEL.2019.2912868

Publication date:
2020

Document Version
Accepted author manuscript, peer reviewed version

IEEE POWER ELECTRONICS REGULAR PAPER

Enhanced Position Sensorless Control Using Bilinear Recursive Least Squares Adaptive Filter for Interior Permanent Magnet Synchronous Motor

Xuan Wu, Sheng Huang, Kan Liu, *Member*, *IEEE*, Kaiyuan Lu, *Member*,*IEEE*, Yashan Hu, Wenli Pan, Xiaoyan Peng

***Abstract*- In the back electromotive force (EMF)-based sensorless control of interior permanent magnet synchronous motor (IPMSM), the inverter nonlinearity and flux linkage spatial harmonics will possibly give rise to (6k±1)th harmonics in the estimated back-EMF, especially the 5th and 7th harmonics. Those harmonics will consequently introduce (6k)th harmonic ripples to the estimated rotor position, especially the 6th harmonic component. In order to solve this problem, a bilinear recursive least squares (BRLS) adaptive filter is proposed and integrated into a sliding mode position observer to suppress the dominant harmonic components in the estimated back-EMF and as a result, the accuracy of the estimated rotor position can be greatly improved. A unique feature of the BRLS adaptive filter is its ability to track and suppress the specified harmonic components in different steady state and dynamic operational conditions. The proposed method can compensate harmonic ripples caused by the inverter nonlinearity and machine spatial harmonics at the same time; this method is also robust to machine parameter variation and the BRLS algorithm itself is machine parameter independent. The implementation of the proposed BRLS filter in the sensorless control of IPMSM is explained in details in this paper. The enhanced drive performances using the BRLS filter have been thoroughly validated in different steady state and dynamic operational conditions on a 1.5kW IPMSM sensorless drive. [1]**

***Index Terms*—Bilinear recursive least squares (BRLS) adaptive filter, interior permanent magnet synchronous motor (IPMSM), position estimation error, position observer, sensorless, sliding-mode observer (SMO).**

I. INTRODUCTION

INTERIOR permanent magnet synchronous motors (IPMSMs) have been widely utilized in various industrial applications due to their superior performances such as high torque to volume ratio, high efficiency, and high power density [1]-[4]. In an IPMSM control system, accurate rotor position information is usually essential, whereas it is still too costly to use a mechanical position sensor which will also increase the system size and reduce its reliability. Alternatively, position sensorless control of IPMSM has been widely studied in numerous research articles [5]-[28]. However, in applications of e.g. high pole-pair number wind power generators, there are still challenges in meeting high steady state and dynamic rotor position estimation accuracy demands when distorted back-EMF caused by flux spatial harmonics and inverter nonlinearity exists.

Position estimation methods for sensorless IPMSM can be mainly divided into two types depending on the operational speed ranges. High-frequency injection methods [5]-[15] are suitable for low and zero speeds and back-EMF-based methods are typically used for medium and high speeds [16]-[28]. The position estimation methods based on the back-EMF model mainly contain the model reference adaptive estimation method, the flux estimation method, and the sliding-mode observer (SMO), etc. Among them, the SMO method is recognized as having good robustness against disturbances, low sensitivity to parameter variations and implementation simplicity. This method has been widely employed in sensorless control of IPMSM at medium and high speeds [23]-[28] and will be used in this paper as well.

However, the estimated back-EMF is often distorted by the dominant fifth and seventh harmonics brought by inverter nonlinearity and flux spatial harmonics; then, the corresponding estimated position will contain a dominant sixth harmonic component, deteriorating the sensorless control performance for IPMSM. Much research has been done to compensate the inverter nonlinearity effects [29]-[34]. For example, in [29] and [30], the voltage difference between the actual and reference voltage caused by inverter nonlinearity is compensated by using a trapezoidal compensation voltage to improve the accuracy of the estimated rotor position. In [32], a simple parameter independent online compensation method is proposed to reduce the effect of the inverter nonlinearity in IPMSM control using measured current waveforms. In [33], the disturbance voltage caused by inverter nonlinearity is calculated by a special back-EMF function and flux linkage increments, and then it is used as a feed-forward component added to the current loop to achieve the compensation. Even though the inverter voltage error is assumed to be

Manuscript received August 06, 2018; revised September 16, 2018, December 04, 2018 and February 13, 2019; accepted April 17, 2019. This work was supported by the Research Fund for the National Science Foundation of China (51707062, 51575167 and 51877075).

Xuan Wu, Yashan Hu and Wenli Pan are with the College of Electrical and Information Engineering at Hunan University, Hunan, China (e-mail: wuxuan24@163.com; hu_ya_shan@sina.com; panwl870@hnu.edu.cn). Sheng Huang is with the Department of Electrical Engineering, Technical University of Denmark, 2800 Kgs. Lyngby. Denmark (e-mail: huang98123@163.com). Kaiyuan Lu is with the Department of Energy Technology at Aalborg University, Aalborg, Denmark (e-mail: klu@et.aau.dk). Kan Liu and Xiaoyan Peng are with the College of Mechanical and Vehicle Engineering at Hunan University, Changsha, China (e-mail: lkan@hnu.edu.cn and xypeng@hnu.edu.cn).Corresponding author: Yashan Hu (e-mail: hu_ya_shan@sina.com).

compensated completely (which is difficult to achieve in practice due to e.g. current sampling delay etc.), spatial flux linkage harmonics caused by non-ideal air gap flux density waveform may also introduce (6k±1)th harmonics to the estimated back-EMF [35]-[36]. In [36], a new model considering the spatial harmonics was established, but offline analysis of the measured back-EMF is required, which increases the implementation complexity. However, for sensorless drives to achieve accurate and less disturbed estimated position, instead of compensating or suppressing the harmonics created by the inverter or the machine, it will be a more straightforward approach to filter out the harmonics contained in the back-EMF signal before it is used for position estimation.

Various (6k±1)th harmonics filtering methods have been proposed in [37]-[45]. Resonant filter, as one of the promising solutions, has been widely used in grid-connected inverter control. But due to the phase angle response characteristic of the resonant filter, its performance is sensitive to the resonant frequency. For variable speed drive applications, it is difficult to track the resonant frequency accurately during speed transients and load torque disturbances. Its performance will then be greatly scarified for variable speed sensorless IPMSM drives. This technique has been subsequently extended in [38] to include a proportional gain to suppress the current harmonics. However, the resonant regulator will tend to degrade the current loop control performance resulting in current overshoot when applied to motor control. In [39], the current harmonic suppression issue in sensorless PMSM drive is attempted by a feed-forward compensation strategy. Although the technique contributes to current harmonic attenuation, its effectiveness depends on the values of system parameters. As another filter type, the adaptive filter has been applied in signal processing applications to enhance the signal and filter out unwanted harmonic components [40]-[41]. Adaptive filter has the ability to track online the change of a specified frequency component caused by changed working conditions [42]-[48]. In implementation, the two common types of adaptive filters are the least mean square (LMS) adaptive filter [42]-[43] and the bilinear recursive least squares (BRLS) adaptive filter [44]-[48]. The performance of harmonic detection accuracy and convergence speed may be improved by using an adaptive step for the LMS adaptive filter [43], but its performance is still sensitive to the change of the parameters. Compared with the LMS adaptive filter, the BRLS adaptive filter is easier to implement requiring less calculation efforts and it has stronger robustness and faster convergence rate.

The BRLS adaptive filter can continuously self-adjust the filter coefficients using the BRLS adaptive algorithm according to the signal characteristics, which forces the system to track the specified harmonic component. It is an effective method to detect and then suppress the harmonic components. Two feedback regulation mechanisms are involved in the BRLS adaptive filter, which improves the harmonic component detection accuracy. In [45], the BRLS adaptive filter is used for the initial alignment of an inertial navigation system, which improves the initial alignment accuracy and ensures a fast convergence rate of the strap down inertial navigation system. In [46], the BRLS adaptive filter has been applied in grid-connected inverter control due to its capability of detecting and suppressing the selected harmonic component. The system was able to estimate the instantaneous symmetrical components of the grid voltage under unbalanced and distorted grid conditions. Application of the BRLS filter to variable speed sensorless drives has been rarely reported yet. It is worth to mention that although the BRLS filter technique is not new, but its adaptive harmonic component tracking and suppressing ability that can bring promising performance improvement when applied for back-EMF based sensorless drives has not been properly studied and reported so far. Reduced harmonic components in the back-EMF can bring reduced position and speed estimation errors, which are important for sensorless drives. Introduction of BRLS filter to a sensorless drive, explaining its realization details and solid experimental validations showing enhanced sensorless drive performance are also the new contributions of this paper.

In this paper, the estimated position error with the (6k)th harmonics caused by the spatial harmonics of flux linkage and the inverter nonlinearity is analyzed first. Then, an enhanced SMO method using the BRLS adaptive filter is employed to detect and suppress the specified harmonics in the estimated back-EMF, reducing consequently the harmonic position error in the estimated rotor position. Both the distortions caused by flux spatial harmonics and inverter nonlinearity can be compensated at the same time. The proposed adaptive compensation method is independent of motor parameters and can enhance the robustness and reduce the sensitivity of the sensorless controller to machine parameter variations. Experimental results confirmed that the proposed method can effectively improve the accuracy of the estimated rotor position and enhance the sensorless control performance of the IPMSM drive.

II. Sensorless Control Based On Sliding Mode Observer

The schematic diagram of the proposed sensorless control for IPMSM is depicted in Fig.1, in which a position observer with BRLS adaptive filter in Fig.2 is employed for suppression of the harmonics contained in the back-EMF. The rotor position is estimated by using the conventional extended back-EMF model of IPMSM in the $\alpha\beta$ reference frame [18], which can be expressed as:

$$\begin{cases} u_\alpha = R_s i_\alpha + L_d \dfrac{d}{dt} i_\alpha + \omega_r (L_d - L_q) i_\beta + e_\alpha \\ u_\beta = R_s i_\beta + L_d \dfrac{d}{dt} i_\beta - \omega_r (L_d - L_q) i_\alpha + e_\beta \end{cases} \tag{1}$$

where $u_\alpha, u_\beta, i_\alpha$ and i_β are the stator voltages and the stator currents in the $\alpha\beta$-axes, respectively; L_d and L_q are the dq-axes inductances; R_S is the stator resistance; ω_r is the electrical sp-

This article has been accepted for publication in a future issue of this journal, but has not been fully edited. Content may change prior to final publication. Citation information: DOI 10.1109/TPEL.2019.2912868, IEEE Transactions on Power Electronics

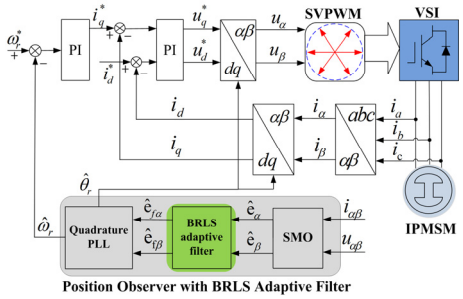

Fig. 1. Back-EMF mode1-based sensorless IPMSM drive.

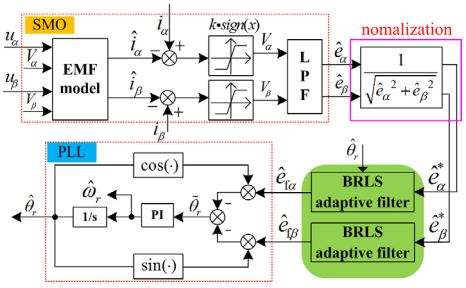

Fig. 2. Position observer based on the proposed BRLS adaptive filter.

-eed and $e_{\alpha\beta}$ is the extended back-EMF defined by:

$$\begin{bmatrix} e_\alpha \\ e_\beta \end{bmatrix} = [(L_d - L_q)(\omega_r i_d - di_q/dt) + \lambda_{mpm}\omega_r] \begin{bmatrix} -\sin\theta_r \\ \cos\theta_r \end{bmatrix} \quad (2)$$

where λ_{mpm} is the permanent magnet flux linkage and θ_r is the rotor electrical position.

Thus, a SMO is designed based on the extended back-EMF model, which can be expressed as:

$$\frac{d}{dt}\begin{bmatrix} \hat{i}_\alpha \\ \hat{i}_\beta \end{bmatrix} = A\begin{bmatrix} \hat{i}_\alpha \\ \hat{i}_\beta \end{bmatrix} + \frac{1}{L_d}\begin{bmatrix} u_\alpha \\ u_\beta \end{bmatrix} - \frac{1}{L_d}\begin{bmatrix} v_\alpha \\ v_\beta \end{bmatrix} \quad (3)$$

where, $v_{\alpha\beta} = \begin{cases} k/\delta \bullet (\hat{i}_{\alpha\beta} - i_{\alpha\beta}), for \left|\hat{i}_{\alpha\beta} - i_{\alpha\beta}\right| < \delta \\ k \bullet sign(\hat{i}_{\alpha\beta} - i_{\alpha\beta}), for \left|\hat{i}_{\alpha\beta} - i_{\alpha\beta}\right| > \delta \end{cases}$, k is the gain of SMO, δ is the boundary layer, "^" denotes the estimated values; $A = \frac{1}{L_d}\begin{bmatrix} -R_s & -(L_d - L_q)\omega_r \\ (L_d - L_q)\omega_r & -R_s \end{bmatrix}$.

Due to the variation of the estimated back-EMF magnitude at different speeds, the normalization of the estimated back-EMF for a quadrature PLL is adopted. The normalized position error can be approximately obtained by:

$$\tilde{\theta}_r \approx \sin\tilde{\theta}_r = \frac{1}{\sqrt{\hat{e}_\alpha^2 + \hat{e}_\beta^2}}(-\hat{e}_{f\alpha}\cos\hat{\theta}_r - \hat{e}_{f\beta}\sin\hat{\theta}_r) \quad (4)$$

where $\hat{e}_{f\alpha}$ and $\hat{e}_{f\beta}$ are the fundamental components of $\hat{e}_\alpha$ and $\hat{e}_\beta$, given by the BRLS adaptive filter. $\hat{e}_\alpha$ and $\hat{e}_\beta$ are the estimated extended back-EMF, which can be obtained from low-pass filtered v_α and v_β signals as:

$$\begin{bmatrix} \hat{e}_\alpha \\ \hat{e}_\beta \end{bmatrix} = \frac{\omega_c}{s + \omega_c}\begin{bmatrix} v_\alpha \\ v_\beta \end{bmatrix} \quad (5)$$

where ω_c is the cut-off frequency of the low-pass filters.

Therefore, the estimated position can be obtained through the quadrature PLL, which can be expressed as:

$$\hat{\theta}_r = \frac{1}{s}(\frac{k_i}{s} + k_p)\tilde{\theta}_r \quad (6)$$

The transfer function of the quadrature PLL with back-EMF normalization can be expressed as:

$$G_{PLL} = \frac{\hat{\theta}_r}{\theta_r} = \frac{k_p s + k_i}{s^2 + k_p s + k_i} \quad (7)$$

In the practical application, both the two poles of (7) are placed in the left region of the real axis. For simplicity, let the two poles overlap at the same point ρ, and then

$$G_{PLL} = \frac{2\rho s + \rho^2}{s^2 + 2\rho s + \rho^2} \quad (8)$$

Hence, $k_p = 2\rho$ and $k_i = \rho^2$. Considering the trade-off between the elimination of the noises and the dynamic performance, the bandwidth of the quadrature PLL should be designed to be comparatively wide.

III. Analysis of the Harmonic in Back-EMF and the Estimated Position

A. Harmonics in the Back-EMF Caused by Inverter Nonlinearity Effects

Due to the inverter nonlinearity, a voltage difference between the reference and the actual value is introduced, which causes stator current distortion [29]. (6k±1)th harmonics in the stator currents will be introduced, which can be written as:

$$\begin{aligned} i_x &= I_1 \sin(\omega_r t + \theta_1 - i \cdot 2\pi/3) \\ &+ \sum_{k=1}^{n} I_{6k\pm1} \sin[\pm(6k\pm1)\omega_r t + \theta_{6k\pm1} - i \cdot 2\pi/3] \end{aligned} \quad (9)$$

where subscript x represents a, b or c phase and correspondingly, the index i is 0, 1 or 2 respectively. I_1, $I_{6k\pm1}$ are the amplitudes of the fundamental, (6k±1)th harmonics in the stator currents, respectively. θ_1, $\theta_{6k\pm1}$ are their corresponding initial phase angles.

Using the reference frame transformation, the stator currents in the dq reference frame can be obtained as:

$$i_d = I_1 \sin\theta_1 + \sum_{k=1}^{n} I_{6k\pm1} \sin(\pm 6k\omega_r + \theta_{6k\pm1}) \quad (10)$$

$$i_q = -I_1 \cos\theta_1 - \sum_{k=1}^{n} I_{6k\pm1} \cos(\pm 6k\omega_r + \theta_{6k\pm1}) \quad (11)$$

Substituting (10) and (11) into (2), the extended back-EMF in the $\alpha\beta$-axes can be expressed by:

$$e_\alpha = (L_d - L_q)\omega_r\{(-I_1\sin\theta_1 + \frac{\lambda_{mpm}}{L_d - L_q})\sin\omega_r t \mp \sum_{k=1}^{n}\frac{6k\mp1}{2}I_{6k\pm1}[\cos(\pm(6k\pm1)\omega_r t + \theta_{6k\pm1}) - \cos(\pm(6k\mp1)\omega_r t + \theta_{6k\pm1})]\} \quad (12)$$

$$e_\beta = (L_d - L_q)\omega_r\{(I_1\sin\theta_1 + \frac{\lambda_{mpm}}{L_d - L_q})\cos\omega_r t \mp \sum_{k=1}^{n}\frac{6k\mp1}{2}I_{6k\pm1}[\sin(\pm(6k\pm1)\omega_r t + \theta_{6k\pm1}) - \sin(\pm(6k\mp1)\omega_r t + \theta_{6k\pm1})]\} \quad (13)$$

It can be seen that there are obvious (6k±1)th harmonic components in the back-EMF, and those harmonics will also exist in the estimated back-EMF obtained by SMO [18]. The presence of the harmonics in the estimated back-EMF, which is consequently used for position estimation, increases the position estimation error.

B. Harmonics of the Back-EMF Caused by Flux Spatial Harmonics

Besides the inverter nonlinearity, the back-EMF distortion due to the flux spatial harmonics can also contribute to increased position estimation error for IPMSM. The flux spatial harmonics may be caused by non-ideal air-gap flux density waveforms [18]. So the back-EMF of IPMSM becomes non-sinusoidal. The flux generated by the permanent magnet can be expressed as

$$\lambda_{m,k}(\theta_r) = \lambda_k\cos(k\theta_r - \frac{2\pi}{3}(m-1)) \quad (14)$$

where λ_k is the amplitude of the fundamental and harmonic flux linkages; m =1, 2, 3 is respectively a, b, c phase and k =1, 2, 3,... is the harmonic order. For the (3k)th harmonics, due to $\lambda_{a,3k} = \lambda_{b,3k} = \lambda_{c,3k}$ the corresponding flux are equal to zero after Clark transformation. So the fifth and seventh harmonic components become dominant harmonics, which will be introduced into the back-EMF due to their relatively large amplitudes [35]-[36].

It is necessary to suppress the harmonics in the estimated back-EMF in order to improve the position estimation accuracy. It is known that the low-pass filter introduced in (5) used in the SMO can suppress high-order harmonics to a certain extent, but it also introduces a phase delay between the estimated and actual back-EMF as illustrated in Fig.3. There is a contrary relationship between the harmonic suppression ability and the phase delay of the low-pass filters, and both of them are related to the cut-off frequency ω_c. It means that for a larger ω_c, there will be a smaller phase delay between the estimated back-EMF and the actual back-EMF but weaker harmonic suppression ability. A smaller phase delay is necessary to improve the estimation accuracy when using the SMO. Usually the cutoff frequency of the SMO is chosen by $\frac{\hat{\omega}_r}{K}$, where $\hat{\omega}_r$ is the estimated electrical angular velocity and K is a constant, with recommended values between 1-2. When

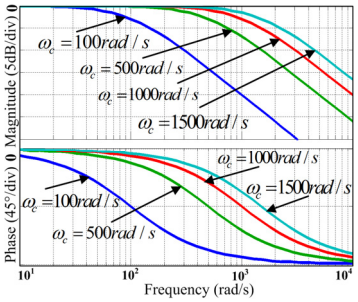

Fig. 3. Relationship between phase angle delay, harmonic suppression ability and cut-off frequency.

the value of K increases, the cutoff frequency ω_c will reduce. So there will be a lager phase delay in the estimated back-EMF once processed by the LPF. In order to reduce the phase delay of the estimated back-EMF, the cutoff frequency ω_c needs to have a relatively larger value than the normal recommended values. In this implementation, K is chosen to be 0.1 for reducing the phase delay in the estimated back-EMF and achieving a good performance for the SMO. Thus the (6k±1)th harmonics in the estimated back-EMF are difficult to be filtered out, especially for the fifth and seventh harmonics.

C. Position Estimation Error Due to the Back-EMF Harmonics

In order to analyze the influences of the (6k±1)th harmonics on the estimated back-EMF and consequently on the estimated rotor position, the estimated back-EMF is re-written as:

$$\begin{cases}\hat{e}_\alpha^* = -e_{f\alpha} - e_{h\alpha}\\ \hat{e}_\beta^* = e_{f\beta} + e_{h\beta}\end{cases} \quad (15)$$

where e_f and e_h denote the fundamental component and (6k±1)th harmonics in the estimated back-EMF, which can be expanded as:

$$\begin{bmatrix}\hat{e}_\alpha^*\\ \hat{e}_\beta^*\end{bmatrix} = \underbrace{\begin{bmatrix}-e_1\sin(\omega_r t + \theta_{r1})\\ e_1\cos(\omega_r t + \theta_{r1})\end{bmatrix}}_{e_f} + \underbrace{\begin{bmatrix}-e_{6k\pm1}\sin(\pm(6k\pm1)\omega_r t + \theta_{r(6k\pm1)})\\ e_{6k\pm1}\cos(\pm(6k\pm1)\omega_r t + \theta_{r(6k\pm1)})\end{bmatrix}}_{e_h} \quad (16)$$

where e_1 and $e_{6k\pm1}$ represent the amplitudes of the fundamental and (6k±1)th harmonic components; θ_{r1} and $\theta_{r(6k\pm1)}$ represent the corresponding initial phase angles, respectively.

Combining (4) with $\hat{\theta}_r = \hat{\omega}_r t + \hat{\theta}_{r1}$, the estimated rotor position error can be obtained as:

This article has been accepted for publication in a future issue of this journal, but has not been fully edited. Content may change prior to final publication. Citation information: DOI 10.1109/TPEL.2019.2912868, IEEE Transactions on Power Electronics

$$\begin{aligned}\tilde{\theta}_{\mathrm{r}} \approx \sin\tilde{\theta}_{\mathrm{r}} &= (-\hat{e}_{\alpha}^{*}\cos\hat{\theta}_{r} - \hat{e}_{\beta}^{*}\sin\hat{\theta}_{r}) \\ &= e_1\sin[(\omega_r - \hat{\omega}_r)t + \theta_{r1} - \hat{\theta}_{\mathrm{r1}}] \\ &+ \sum_{k=1}^{n} e_{6k\pm1}\sin[(\pm(6k\pm1)\omega_r - \hat{\omega}_r)t + \theta_{r(6k\pm1)} - \hat{\theta}_{r1}]\end{aligned} \tag{17}$$

Since ω_r is approximately equal to $\hat{\omega}_r$, so (17) can be re-written as:

$$\begin{aligned}\tilde{\theta}_{\mathrm{r}} \approx \sin\tilde{\theta}_{\mathrm{r}} &= -\hat{e}_{\alpha}^{*}\cos\hat{\theta}_{r} - \hat{e}_{\beta}^{*}\sin\hat{\theta}_{r} \\ &= e_1\sin[(\omega_r - \hat{\omega}_r)t + \theta_{r1} - \hat{\theta}_{\mathrm{r1}}] \\ &+ \sum_{k=1}^{n} e_{6k-1}\sin[(-(6k)\hat{\omega}_r t + \theta_{r(6k-1)} - \hat{\theta}_{r1}] \\ &+ \sum_{k=1}^{n} e_{6k+1}\sin[(+(6k)\hat{\omega}_r t + \theta_{r(6k+1)} - \hat{\theta}_{r1}]\}\end{aligned} \tag{18}$$

From the second term in (18), it can be observed that the (6k)th harmonics are introduced into the position estimation error. The estimated position is obtained from a quadrature PLL with the position estimation error containing (6k)th harmonics as the input signal. Therefore, the estimated rotor position also contains (6k)th harmonic fluctuations.

In order to improve the accuracy of the estimated position, the inverter nonlinearity that causes voltage distortion should be compensated. In this paper, the trapezoidal voltage compensation method as proposed in [29] is utilized to compensate the distorted voltage. The method reported in [29] uses harmonic current detection and closed-loop current control to suppress the inverter voltage error and has achieved good results. However, with this compensation, the (6k)th harmonic ripple in the estimated rotor position still exists. This can be observed from the experimental results under sensorless control given in Fig.4, where the position estimation error at 600r/min with 50% rated load is shown. The cutoff frequency of the LPF is 1300 rad/s in Fig.4. Fig.4(a), (b) shows the results without any compensation and with inverter nonlinear voltage error compensation using the method reported in [29], respectively. There are obvious harmonic ripples in the estimated rotor position and sixth harmonic component in the estimated position error. So to further reduce the dominant (6k)th harmonics in the estimated position, other efforts are required.

VI. Harmonic Diminish Method in the Estimated Back-EMF Using BRLS Filter

The (6k±1)th harmonic components in the estimated back-EMF can reduce the estimation accuracy and deteriorate the performance of an IPMSM sensorless drive. The bilinear recursive least squares (BRLS) adaptive filter is an effective method to detect harmonics, which has been widely used in signal enhancement [45]. The BRLS filter can adaptively track harmonics in the estimated back-EMF by online updating the filter coefficients using the BRLS adaptive algorithm, and the detected harmonics can be filtered out to obtain the fundamental component of the estimated back-EMF.

It can be noted that there are obvious sixth harmonic ripple in the estimated rotor position error, namely the index *k* of the (6k)th is 1. The higher (6k)th (k>=2) harmonics such as the twelfth harmonic will have smaller amplitudes and their effects on the position estimation accuracy can be neglected. So the sixth harmonic is considered as the dominant harmonic component in the estimated position error. Correspondingly, the fifth and seventh harmonic components in the estimated back-EMF are the dominant harmonic components. This paper will therefore consider only filtering out the fifth and seventh harmonic components in the estimated back-EMF and the sixth harmonic ripple in the estimated rotor position.

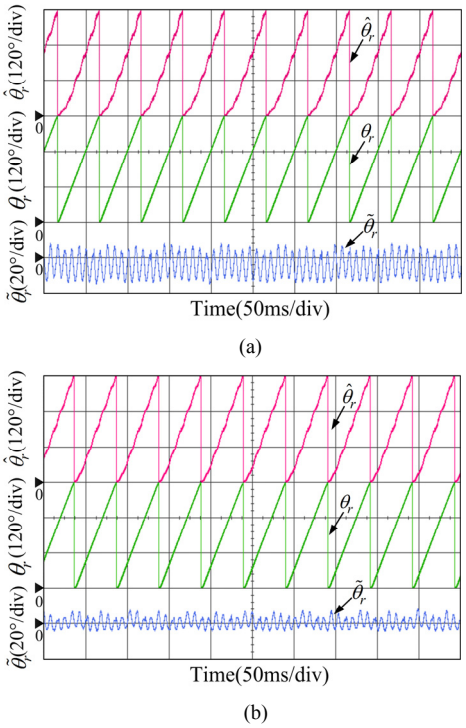

Fig. 4. Experimental results of the actual rotor position, the estimated rotor position and the estimated rotor position error with sensorless control at 600 r/min under 50% rated load. (a) Without any compensation; (b) With inverter nonlinear voltage error compensation.

A. Principle of BRLS Adaptive Position Estimation Error Suppression

Fig.5 gives the implementation block diagram of the BRLS adaptive filter for detecting and suppressing harmonics. *d(k)* denotes the original signal consisting of the fundamental signal *f(k)* and the harmonic signal *h(k)*. *x(k)* denotes the input signal related to high-order harmonic components. Through iterative computation, the filter's output signal *y(k)* can be obtained through the input signal *x(k)* processed by BRLS adaptive algorithm. After the adaptive filter converges, the output signal *y(k)* can track the actual high-order harmonic components *h(k)*. Then the desired fundamental component *f(k)* can be obtained by subtracting *y(k)* from *d(k)*, namely the error signal *e(k)*. Because coefficients of the adaptive filter can be adjusted by BRLS adaptive algorithm, the output signal y(k)

This article has been accepted for publication in a future issue of this journal, but has not been fully edited. Content may change prior to final publication. Citation information: DOI 10.1109/TPEL.2019.2912868, IEEE Transactions on Power Electronics

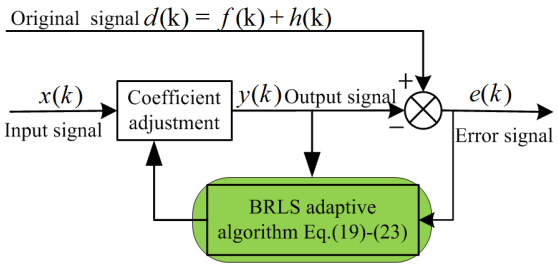

Fig. 5. Structure of harmonic detection and suppression by using adaptive filter based on the BRLS adaptive algorithm.

can be adaptively changed following the change of the harmonic components to achieve a robust harmonic filtering performance. Meanwhile, compared with the LMS adaptive filter, the BRLS adaptive filter uses a less filter order, which reduces the computational complexity and delay. In addition, the BRLS adaptive filter has better estimation accuracy by introducing *y(k)* and *e(k)* as feedback signals inside the adaptive mechanism.

The fifth and seventh harmonics in the estimated back-EMF of the $\alpha\beta$-axes will be converted into the sixth harmonic of the estimated back-EMF in the *dq*-axes through Park transformation. Besides the implementation structure shown in Fig.1, the BRLS filter may also be implemented in the *dq*-reference frame. But this requires extra reference frame transformations and the rotor position information, which contains position estimation errors and is to be estimated later on by using the filtered back-EMF, is needed. In this paper, the BRLS filters are chosen to be implemented in the $\alpha\beta$-reference frame.

The BRLS adaptive filter will be utilized to suppress the fifth and seventh harmonic components in the estimated back-EMF. In the following, filtering out the fifth and seventh harmonic components of the estimated back-EMF in the α-axis is taken as an example to explain the application of the BRLS adaptive filter in suppressing the estimated back-EMF harmonics. The signal processing process of the BRLS adaptive filter used for position estimation is illustrated in Fig.6.

Fig.6(a) illustrates how the BRLS filter estimates and removes the 5th and 7th harmonics for the α-component of the estimated back-EMF obtained from SMO. Fig.6(a) shows that the "BRLS adaptive algorithm" is used to estimate the 5th and 7th harmonics and then those components are subtracted from the original back-EMF signal given by the SMO in the output. The implementation details of the "BRLS adaptive algorithm" is given in Fig.6(b), taking the block with "$\sin(-5\hat{\theta}_r)$" as the input and "*y1(k)*" as the output as an illustration example.

The BRLS adaptive algorithm illustrated in Fig.6(b) is used to update the filter's coefficients based on e.g. the 5th harmonic component re-constructed from the estimated position and the output of this BRLS filter. This kind of feedback loop is needed, so the adaptive filter based on BRLS adaptive algorithm can track the specified harmonic compone-

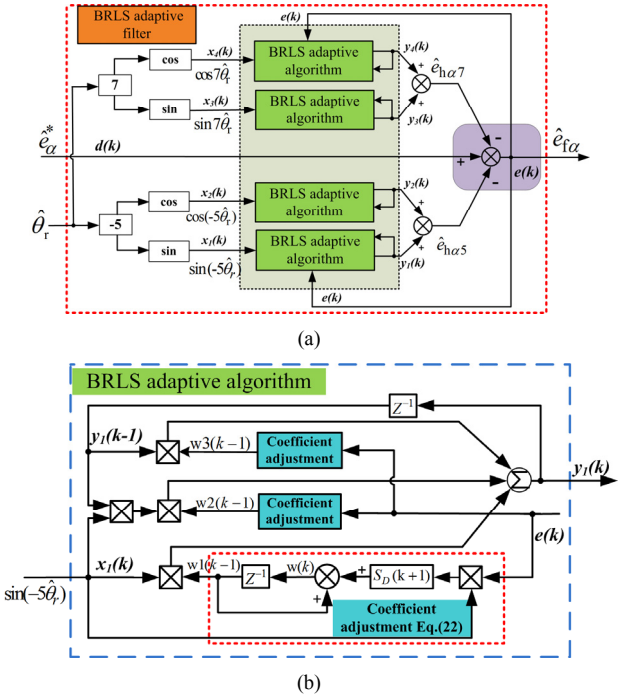

Fig. 6. Structure of the proposed adaptive filter using the BRLS adaptive algorithm to cancel the position harmonic error. (a) Whole frame diagram of suppressing harmonics in estimated back-EMF using adaptive filter based on the BRLS adaptive algorithm; (b) Detailed diagram of BRLS adaptive algorithm.

-nts contained in the estimated back-EMF.

The normalized estimated back-EMF, i.e., $\hat{e}_\alpha^*$ and $\hat{e}_\beta^*$ sever as the original signal *d(k)*, which contains the fundamental back-EMF $\hat{e}_f$ and the fifth and seventh harmonic components $\hat{e}_h$. The input signals *x(k)* are sine and cosine functions of the fifth and seventh of the estimated rotor position $\hat{\theta}_r$, i.e., $\sin(-5\hat{\theta}_r)$, $\cos(-5\hat{\theta}_r)$, $\sin(7\hat{\theta}_r)$, and $\cos(7\hat{\theta}_r)$. These signals will be used in the harmonic information vector $\Phi(k)$. Meanwhile, the output signal *y(k)* is also introduced into the $\Phi(k)$ to enhance the filtering performance of the BRLS adaptive filter. The harmonic information vector $\Phi(k)$ can be obtained by:

$$\phi(k) = [x(k)\ \ y(k-1)\ \ x(k)y(k-1)] \tag{19}$$

The sum of the product of the harmonic information vector $\Phi(k)$ and the filter coefficient vector *w(k)* forms the output signal *y(k)*. Based on the signal enhancement principle, the output signal *y(k)* is equal to the corresponding harmonics $\hat{e}_{h\alpha\beta}$, i.e., $\hat{e}_{5\alpha}$, $\hat{e}_{7\alpha}$, when the BRLS adaptive filter converges. Thus for any harmonic information vector $\Phi(k)$, the output signal can be calculated as:

$$\hat{e}_{h\alpha\beta} \approx y(k) = \phi^T(k)w(k) = \sum_{n=1}\phi_n(k)w_n(k) \tag{20}$$

The desired fundamental component in the estimated back-EMF can be derived directly from the error signal *e(k)* , which is obtained by subtracting the output $\hat{e}_{h\alpha\beta}$ from the original signal $\hat{e}^*_{\alpha\beta}$ and is expressed as follows:

$$\hat{e}_{f\alpha\beta} \approx e(k) = \hat{e}^*_{\alpha\beta} - y(k) \tag{21}$$

To allow the BRLS adaptive filter for detecting and filtering out the fifth and seventh harmonic components in the estimated back-EMF, the filter coefficient are on-line updated based on the harmonic characteristics in the estimated back-EMF.

The filter coefficient updating formula of the BRLS adaptive algorithm is described as follows:

$$w(k+1) = w(k) + S_D(k+1)\phi(k)e(k) \tag{22}$$

where the intermediate vector $S_D(k)$ is given as:

$$S_D(k+1) = \frac{1}{\lambda}\left[S_D(k) - \frac{S_D(k)\phi(k)\phi^T(k)S_D(k)}{\lambda + \phi^T(k)S_D(k)\phi(k)} \right] \tag{23}$$

where λ is the forgetting factor. In practical applications, λ is usually a positive constant, which is close to 1, however less than 1, i.e. 0<<λ<1.

Considering the effect of (6k±1)th harmonics, the high-order harmonic components of the back-EMF in (12) can be re-written as:

$$\begin{aligned} e_h &= e_{6k\pm1}\sin[(6k\pm1)\omega_r t + \theta_{r(6k\pm1)})] \\ &= (e_{6k\pm1}\cos\theta_{r(6k\pm1)})\sin((6k\pm1)\omega_r t) \\ &+ (e_{6k\pm1}\sin\theta_{r(6k\pm1)})\cos((6k\pm1)\omega_r t) \end{aligned} \tag{24}$$

In the vector form, it becomes:

$$e_h = [e_{6k\pm1}\cos\theta_{r(6k\pm1)} \;\; e_{6k\pm1}\sin\theta_{r(6k\pm1)}]\begin{bmatrix}\sin((6k\pm1)\omega_r t)\\ \cos((6k\pm1)\omega_r t)\end{bmatrix} \tag{25}$$

Through the aforementioned analysis and comparison of (15), (16) and (21), it can be seen that the BRLS adaptive filter not only uses $\sin(-5\hat{\theta}_r)$, $\sin(7\hat{\theta}_r)$ and $\cos(-5\hat{\theta}_r)$, $\cos(7\hat{\theta}_r)$ as the references in the BRLS adaptive harmonic information vector ***Φ(k)***, but also feeds the output signal *y(k)* to the ***Φ(k)*** as the feedback signal; so the output *y(k)* can more accurately track and compensate back-EMF high-order harmonics, especially the fifth and seventh components caused by machine spatial flux linkage harmonics and inverter nonlinearity.

B. Analysis of Stability

According to the study carried in [48], the BRLS adaptive filter is stable if the time average of the squared estimation error *e(k)* is bounded whenever the original signal *d(k)* is stable. That means that the BRLS adaptive filter provides a stable output whenever the original signal is stable, i.e. $\frac{1}{n+1}\sum_{k=1}^{n} e^2(k)$ is bounded whenever $\frac{1}{n+1}\sum_{k=1}^{n} d^2(k)$ is bounded. In this paper, *d(k)* is the original signal, namely $\hat{e}^*_{\alpha\beta}$ obtained from the SMO; *e(k)* is the error signal, which is equal to the fundamental back-EMF component $e_{f\alpha\beta}$.

On the basis of (16) , it can be seen that:

$$\begin{aligned} \frac{1}{n+1}\sum_{k=1}^{n} d^2(k) &= \frac{1}{n+1}\sum_{k=1}^{n}(\hat{e}^*_{\alpha\beta})^2 \\ &\le \frac{n}{n+1}(e_1^2 + e_{6k\pm1}^2) < e_1^2 + e_{6k\pm1}^2 \end{aligned} \tag{26}$$

$$\frac{1}{n+1}\sum_{k=1}^{n} e^2(k) \approx \frac{1}{n+1}\sum_{k=1}^{n} e_{f\alpha\beta}^2 \le \frac{n}{n+1}(e_1^2) < e_1^2 \tag{27}$$

From (26) and (27), both of the $\hat{e}^*_{\alpha\beta}$ and $e_{f\alpha\beta}$ are bounded at all time. The time average of the $e_{f\alpha\beta}$ is bounded whenever $\hat{e}^*_{\alpha\beta}$ is bounded. This ensures the stability of the BRLS adaptive filter applied to the position observer for sensorless drives.

C. Analysis of Parameters Selection

In practical implementation, the w(k) and $S_D(k)$ need to be initialized as follows:

$$\begin{aligned} w(k) &= 0 \\ S_D(k) &= \sigma I \end{aligned} \tag{28}$$

where *I* is the unit matrix, and the coefficient of *I* is σ, which is a positive constant. In the BRLS adaptive filter, the selection of σ is based on the ratio of the fundamental signal to the harmonic signal, i.e., the signal-to-noise ratio. Larger signal-to-noise ratio corresponds to a larger value of σ, and smaller signal-to-noise ratio corresponds to a smaller value of σ. Compared with the fundamental back-EMF, the fifth and seventh harmonic components in the estimated back-EMF is relatively small. The total harmonic distortion (THD) is 8.08%. Thus, the σ is chosen to be 0.01.

Meanwhile, the introduction of λin the coefficient adjustment process is used to increase the weight of the current harmonic information vector ***Φ(k)***, which can make the output signal *y(k)* adaptively track the harmonic components. The coefficient λ will directly affect the convergence and the harmonic detection capability. A large forgetting factor λ leads to slow coefficient updating and convergence speed, but good performance of harmonic detection and low misadjustment. On the contrary, a small forgetting factor λ may give a fast convergence speed, but the misadjustment is increased and the adaptive filter sacrifices its harmonic detection accuracy. In general, the forgetting factor λ is very close to 1 and λ can be set to $0.97<\lambda<1$ to avoid undesired divergence [49]. To balance the convergence rate and harmonic detection accuracy, λ is set to be 0.9993.

V. EXPERIMENTAL RESULTS

The proposed sensorless control strategy has been verified on a 1.5kW IPMSM sensorless vector controlled drive. The IPMSM has 4-pole, 12-slot construction, with concentrated windings. The rated parameters of the IPMSM are listed in

This article has been accepted for publication in a future issue of this journal, but has not been fully edited. Content may change prior to final publication. Citation information: DOI 10.1109/TPEL.2019.2912868, IEEE Transactions on Power Electronics

Table I. The experiment setup is depicted in Fig.7. An induction motor is mechanically coupled to the IPMSM to produce the load torque. The dead time of the inverter is 4.3 us. An incremental encoder (PENON-K3808G) is employed to acquire the actual position that is solely used for comparison and not for control purposes. All the experimental results were achieved with the IPMSM operating at sensorless control.

The 32-bit fixed-point DSP family, TMS320F2808 with 100 MHz, is used for digital control of the motor. In the drive for test, the PWM carrier frequency of the inverter is set to be 5 kHz. The IQ math Library is adopted to realize floating-point algorithm from the fixed-point code. The code composing tool is Code Composer Studio 3.3 (CCS3.3). The calculation time of the quadrature PLL based sliding-mode observer with the BRLS adaptive filter algorithm is 18.5μs. The implementation flowchart of the IPMSM drive based on the proposed BRLS adaptive filter is presented in Fig.7(e).

The effectiveness of the proposed method is verified through comparisons with the inverter nonlinearity compensation method reported in [29], because both of them can suppress the harmonics in the back-EMF used for position estimation. In addition, the BRLS filter is compared to another adaptive filter (LMS adaptive filter [43]), demonstrating its fast convergence speed and strong robustness. Three parts of experimental results are given to verify the effectiveness of the proposed approach. The control performances of the proposed method are evaluated from the total harmonic distortion (THD), the operation range, the convergence time and the instantaneous peak-to-peak value of the estimated position error in different operating conditions.

A. Experimental Results at Steady State Using the Proposed Method

Fig.8 gives the experimental results of the estimated back-EMF and its fast Fourier transform (FFT) results at 900 r/min under 50% rated load. Fig.8 (a), (b), (c) ,(d) show the experimental results without any compensation, with the inverter nonlinearity compensation, with the LMS adaptive filter and with the BRLS adaptive filter, respectively. It can be seen that the eleventh and thirteenth harmonics can be neglected due to their small magnitudes. So the focus is laid on the fifth and seventh harmonic components in the estimated back-EMF. The total harmonic distortion (THD) is 8.3%, 6.1%, 2.4%, 2.3% respectively for the corresponding compensation strategies aforementioned. From the experimental results, it can be noted clearly that, the fifth and seventh harmonic components are effectively suppressed using the BRLS adaptive filter and the estimated back-EMF waveform becomes more sinusoidal (Fig.8(d)). By compensating the inverter nonlinearity, the estimated back-EMF still contains fifth and seventh harmonics.

Fig.8(c) gives the experimental results with the LMS adaptive filter [42] for comparison, whose filter order is four in order to achieve a good harmonics suppression ability. The method with the LMS adaptive filter can also suppress harmonics in the estimated back-EMF and reduce the THD to 2.4%. The steady-state performances of the LMS and BRLS adaptive filters are similar; both of them have good steady-state performances in reducing harmonic fluctuations contained in the estimated position error. However, the needed BRLS adaptive filter order is only two, which can obtain the

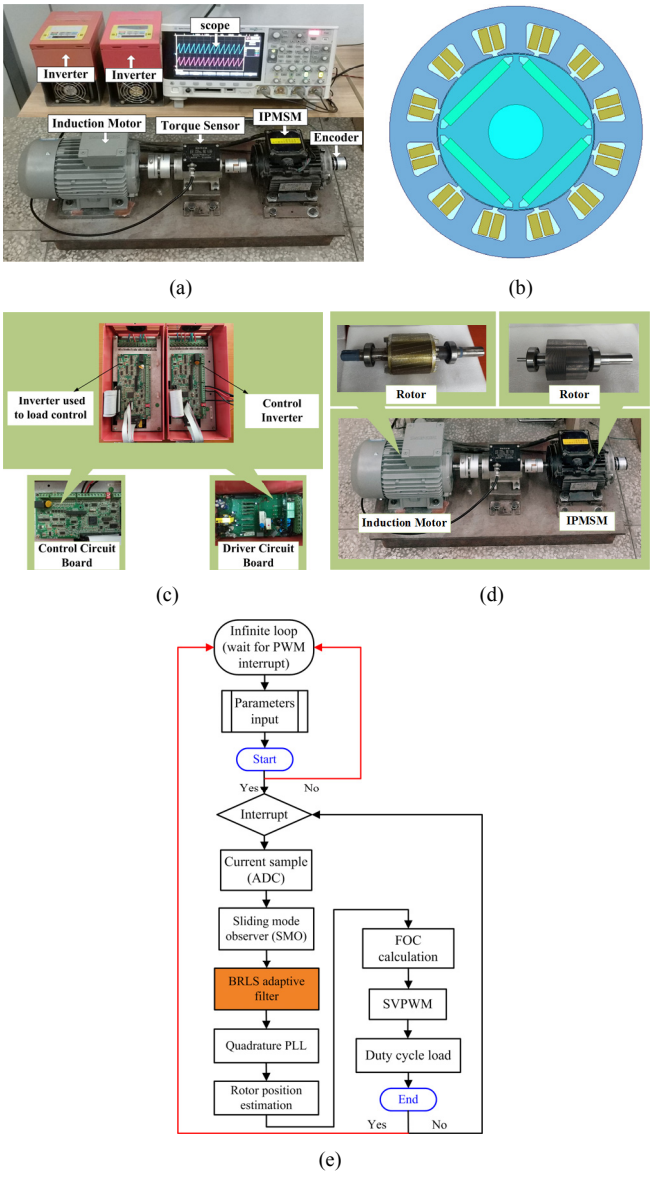

Fig. 7. Experimental platform of 1.5kW IPMSM control system. (a) The whole experimental test; (b) Structure of the tested IPMSM; (c) The inverter for control platform; (d) The drive motors platform; (e) Software data flow of the IPMSM drive based on the proposed BRLS adaptive filter.

TABLE I
PARAMETERS OF THE IPMSM PROTOTYPE

Parameters	Values	Parameters	Values
Rated power /kW	1.5	Rated torque/N.m	4.8
Rated voltage /V	380	Number of pole pairs	2
Rated current /A	2.7	*D*-axes inductance/mH	17.81
Rated speed /(r/min)	3000	*Q*-axes inductance/mH	26.72
Stator resistance / Ω	2.2	Rotor flux linkage /Wb	0.425

This article has been accepted for publication in a future issue of this journal, but has not been fully edited. Content may change prior to final publication. Citation information: DOI 10.1109/TPEL.2019.2912868, IEEE Transactions on Power Electronics

same harmonic suppression performance as that offered by the LMS adaptive filter. The lower filter order makes the BRLS adaptive filter suitable for low computational burden implementations.

The experimental results of the real position, the estimated position, and the estimated position error are given at 900 r/min with 50% rated load in Fig.9. Fig.9 (a), (b), (c), (d) give

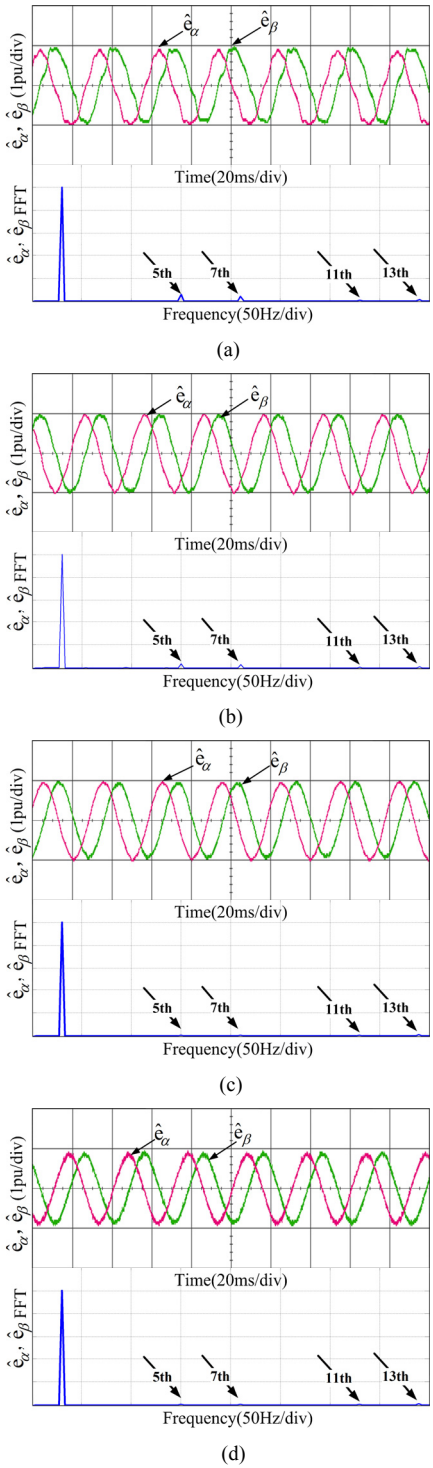

Fig. 8. Experimental results of estimated back-EMF at 900 r/min under 50% rated load. (a) Without any compensation; (b) With the inverter nonlinear voltage error compensation; (c) With the LMS adaptive filter; (d) With the BRLS adaptive filter.

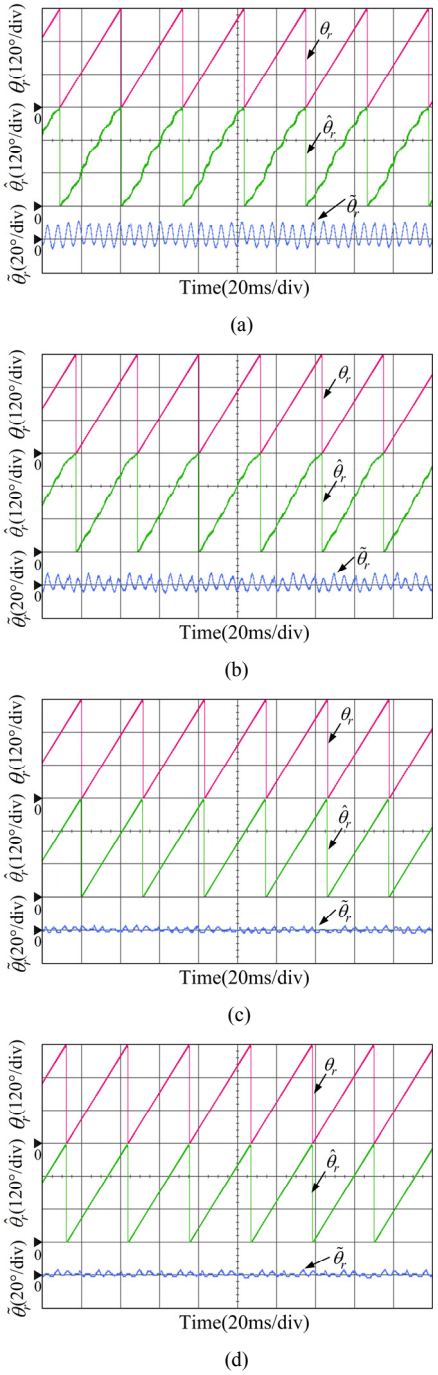

Fig. 9. Experimental results of the estimated rotor position at 900 r/min under 50% rated load. (a) Without any compensation; (b) With the inverter nonlinear voltage error compensation; (c) With the LMS adaptive filter; (d) With the BRLS adaptive filter.

This article has been accepted for publication in a future issue of this journal, but has not been fully edited. Content may change prior to final publication. Citation information: DOI 10.1109/TPEL.2019.2912868, IEEE Transactions on Power Electronics

the experimental results without any compensation, with the inverter nonlinearity compensation, with the LMS adaptive filter and with the BRLS adaptive filter, respectively. Since the adaptive filter is disabled, the harmonics in the estimated back-EMF cannot be filtered, and harmonics especially the fifth and seventh components exist in the estimated back-EMF

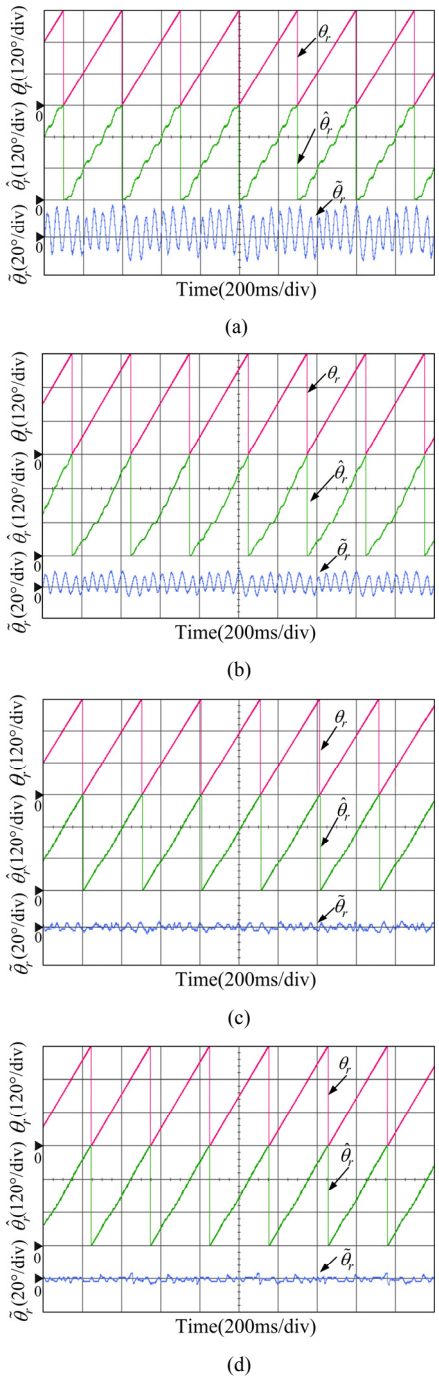

Fig. 10. Experimental results of the estimated rotor position in low-speed at 100r/min under 50% rated load. (a) Without any compensation; (b) With the inverter nonlinear voltage error compensation; (c) With the LMS adaptive filter; (d) With the BRLS adaptive filter.

in Fig.9(a) and Fig.9(b). The instantaneous peak-to-peak value of the estimated position error, obtained by subtracting the actual position from the estimated position, contains sixth pulsation with inverter nonlinear voltage error compensated (Fig.9(b)). The harmonics especially the sixth can be almost diminished with the BRLS adaptive filter (Fig.9(d)) and the estimated position becomes much smooth. With the LMS adaptive filter (Fig.9(c)), the estimated position error can also be reduced. The harmonic ripples of the estimated position error arrive at 11.2°, 6.5°, 3.4°, 3.4° respectively for the different compensation strategies aforementioned.

In the low speed region, the effect of the inverter nonlinearity becomes more obvious and the back-EMF amplitude decreases as the speed decreases. Fig.10 gives experimental results of the estimated rotor position under 50% rated load at 100 r/min, which corresponds to 3.33% of the rated speed. As can be seen, the estimated rotor position is heavily distorted with the sixth harmonic ripple reaching 16.5°in Fig.10(a). The position estimation error is still large, reaching 11.2°with the inverter nonlinearity compensated in Fig.10(b). On the contrary, by using the proposed BRLS adaptive filter (Fig.10(d)), the estimated rotor position offers good estimation accuracy, with a small harmonic ripple of 3.7° in the estimated position error. It can be noted that the proposed BRLS adaptive filter can effectively improve the accuracy of the estimated position even at low speeds and it exhibits consistent performance at different operation speeds. The LMS adaptive filter (Fig.10(c)) can also suppress the harmonic ripples in the estimated position error in steady state.

Fig.11 shows the experimental results at 3000 r/min (rated speed) under 100% rated load. In Fig.11(a) and Fig.11(b), clear sixth pulsation exists in the estimated position. The harmonic components are reduced but are still not small after inverter nonlinear voltage error compensation (Fig.11(b)). The sixth harmonic component in the estimated position can be almost diminished with the help of the BRLS adaptive filter (Fig.11(d)), and the estimated position becomes more smoother and the phase-*a* current becomes more sinusoidal. The LMS adaptive filter is also able to filter out the harmonic contained in the estimated position and reduce the estimated position error as shown in Fig.11(c) in this steady state.

B. Experimental Comparison of Convergence for the BRLS and LMS Adaptive filter

After comparing the steady performance, the convergence and dynamic performances are compared. Fig.12 shows the convergence comparison of the BRLS and LMS adaptive filters. Fig.13 and Fig.14 show the dynamic performance comparison of the BRLS and LMS adaptive filters.

Fig.12 gives the experimental results of the sum of the estimated fifth and seventh harmonics and the estimated rotor position before and after using the BRLS adaptive filter and the LMS adaptive filter at 900 r/min under 50% rated load. Both of the two adaptive filters are enabled at 2.5s. It can be seen that it takes 0.6s for the BRLS filter to achieve convergence after being activated; while for the LMS adaptive filter, it takes about 1.6 s to achieve convergence. In steady

This article has been accepted for publication in a future issue of this journal, but has not been fully edited. Content may change prior to final publication. Citation information: DOI 10.1109/TPEL.2019.2912868, IEEE Transactions on Power Electronics

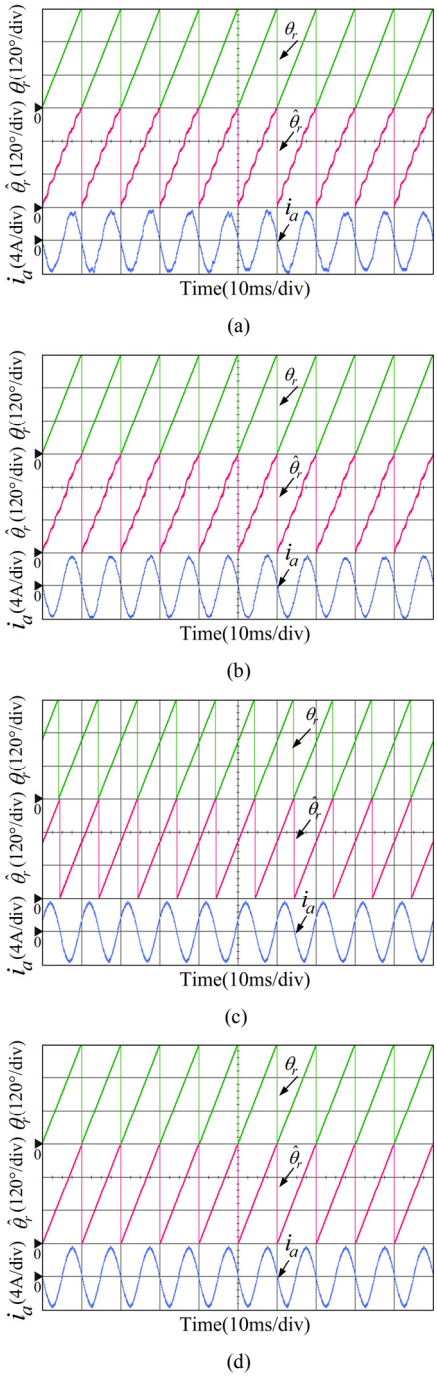

Fig. 11. Experimental results of the estimated rotor position at 3000 r/min under 100% rated load. (a) Without any compensation; (b) With the inverter nonlinear voltage error compensation; (c) With the LMS adaptive filter; (d) With the BRLS adaptive filter.

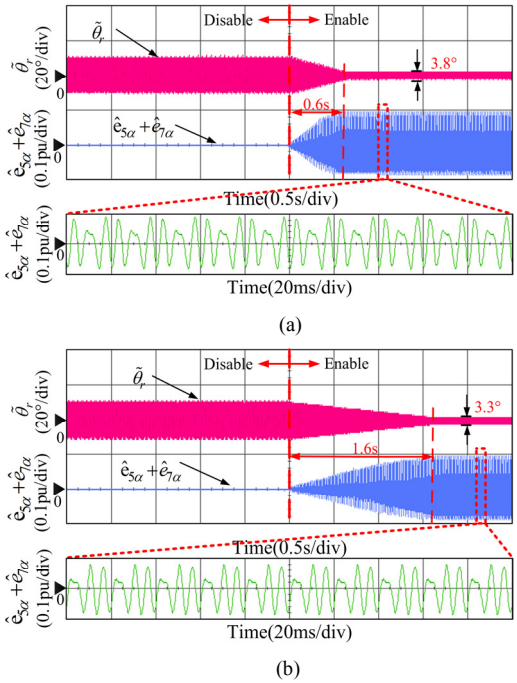

Fig. 12. Experimental results of the estimated position error and the sum of the estimated fifth and seventh harmonics at 900 r/min under 50% rated load. (a) Using the BRLS adaptive filter; (b) Using the LMS adaptive filter.

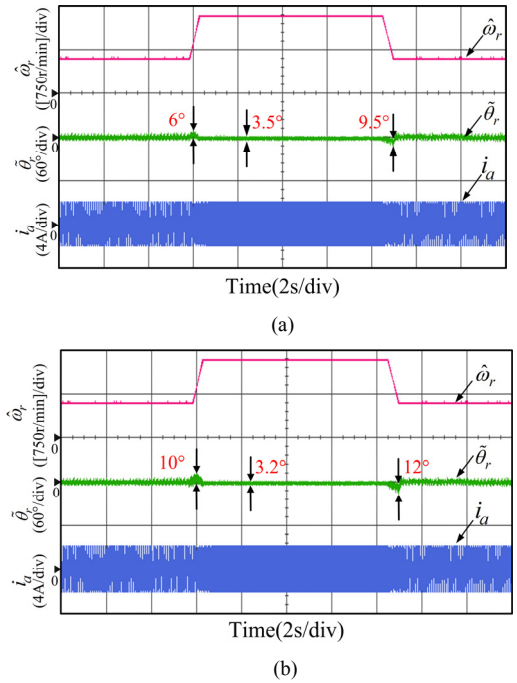

Fig. 13. Experimental comparison at acceleration and deceleration with the BRLS and LMS adaptive filter under 50% rated load. (a) Using the BRLS adaptive filter; (b) Using the LMS adaptive filter.

state, the estimated position error is reduced from 11.7° (no BRLS filter) to 3.8° (with BRLS filter). With the LMS adaptive filter, the estimated position is reduced to 3.3°. The LMS achieves slightly smaller estimated position error but the difference to that given by the BRLS filter is small.

The convergence will directly affect the dynamic response of the IPMSM. Since the BRLS adaptive algorithm converges faster than the LMS adaptive algorithm, the BRLS adaptive

This article has been accepted for publication in a future issue of this journal, but has not been fully edited. Content may change prior to final publication. Citation information: DOI 10.1109/TPEL.2019.2912868, IEEE Transactions on Power Electronics

filter has better dynamic performance. This is confirmed by the experimental results given below.

Fig.13 compares the estimated position error for the BRLS and LMS adaptive filter in speed acceleration and deceleration transients. It may be observed that for the BRLS adaptive filter, the drive undergoes smaller estimated position error before reaching a new steady condition after acceleration and the value of this transient error is almost doubled when using the LMS adaptive filter under the same condition. Similar performances can be observed in the speed deceleration transient. The BRLS adaptive filter can track the speed with a smaller estimated error while both filters can achieve small and very close steady state position and speed estimation errors.

Fig.14 gives the transient experimental results while the drive experiences step load torque change from 20% to 100% rated torque and from 100% to 20% rated torque for those two filters, respectively. From the experimental results, it may be observed that the BRLS and LMS filters have similar steady state estimated position and speed errors but the BRLS adaptive filter needs around only half of the time that is needed for the LMS adaptive filter to reach a new steady state condition. The BRLS adaptive filter can track the load torque change in a faster way.

Considering the advantage of fast convergence ability of the BRLS adaptive filter which results in fast dynamic responses, similar steady state performance when compared with the LMS adaptive filter, and simpler implementation of the BRLS filter than the LMS filter, the BRLS adaptive filter is therefore preferred for this application.

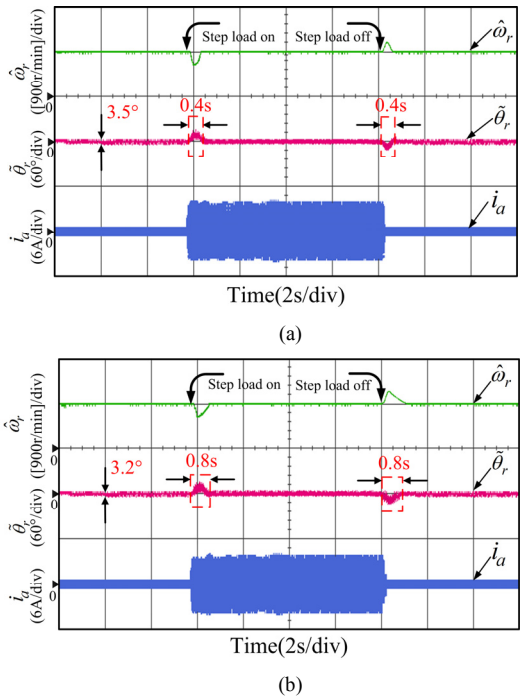

Fig. 14. Experimental comparison with step load torque changes using the BRLS and LMS adaptive filters under 900 r/min. (a) Using the BRLS adaptive filter; (b) Using the LMS adaptive filter.

C. Experimental Results of Control Performance

Fig.15 gives the drive performance comparison at 900 r/min under 50% rated load. From top to bottom, q, d-axes current and phase-a current are given. It can be noted that the ripples

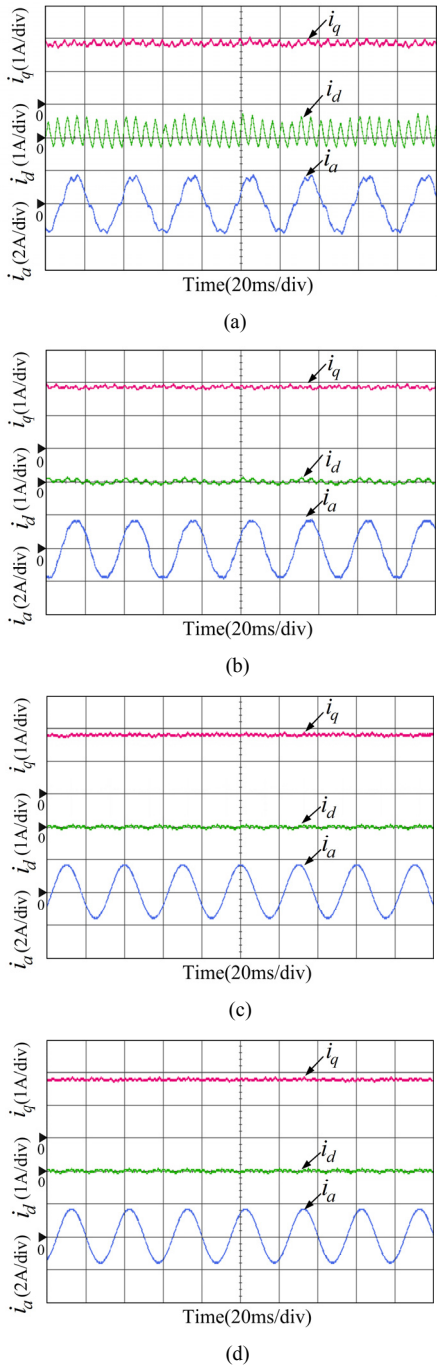

Fig. 15. Control performance experimental results at 900 r/min with 50% rated load. (a) Without any compensation; (b) With the inverter nonlinear voltage error compensation; (c) With the LMS adaptive filter; (d) With the BRLS adaptive filter.

This article has been accepted for publication in a future issue of this journal, but has not been fully edited. Content may change prior to final publication. Citation information: DOI 10.1109/TPEL.2019.2912868, IEEE Transactions on Power Electronics

of i_d, i_q, i_a are reduced obviously by using the BRLS adaptive filter (Fig.15(d)) when compared to the situations without any compensation (Fig.15(a)), and with inverter nonlinearity compensation only (Fig.15(b)). It can be noted that harmonic ripples existing in the estimated position can be reduced by using the BRLS adaptive filter. Using a smoother position in the reference frame transformation will result in smoother d-, q-axis currents, which contributes to less ripples in the speed and torque. Since the steady-state performance of the LMS and BRLS adaptive filter is similar, the ripples of i_d, i_q, i_a are also reduced with the LMS adaptive filter (Fig.15(c)).

Fig.16 gives the estimated position error at different operating conditions. It can be noted that the maximum estimated position error ripple is 13.9°, obtained by the SMO without any compensation (Fig.16(a)); the inverter nonlinear voltage error compensation can reduce the maximum estimated position error to 8.8° in Fig.16(b), but the error is still large. However, the position error obtained by the BRLS adaptive filter can be reduced to 4.2° in Fig.16(d). This clearly demonstrates that the BRLS adaptive filter can suppress the harmonic fluctuations in the estimated position effectively, and offers high robustness to harmonic amplitude variations experienced at different operation conditions. Compared with

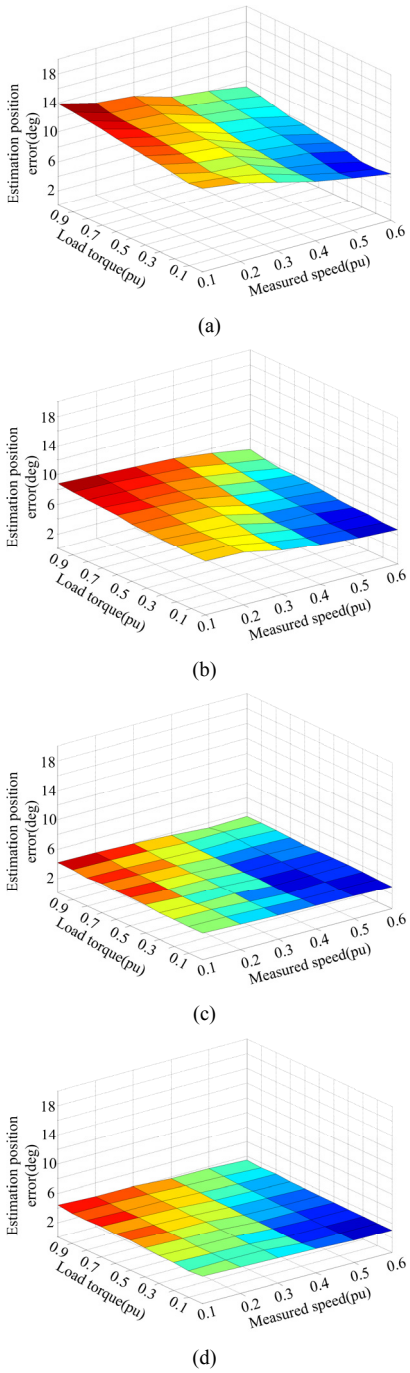

Fig. 16. Estimation position errors with different operating conditions. (a) Without any compensation; (b) With the inverter nonlinear voltage error compensation; (c) With the LMS adaptive filter; (d) With the BRLS adaptive filter.

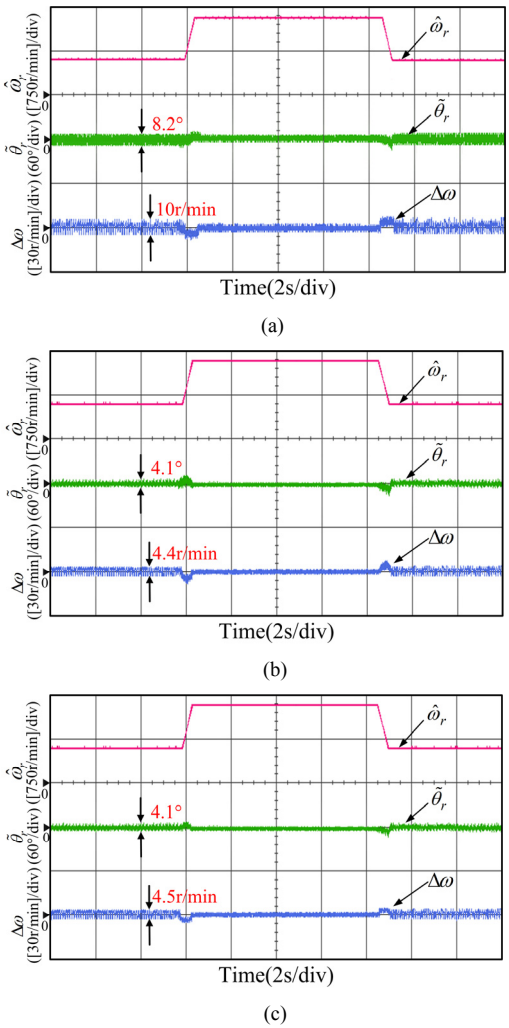

Fig. 17. Experimental results of the position and speed estimation errors with 50% rated load under operating condition of acceleration and deceleration. (a) With the inverter nonlinear voltage error compensation; (b) With the LMS adaptive filter; (c) With the BRLS adaptive filter.

This article has been accepted for publication in a future issue of this journal, but has not been fully edited. Content may change prior to final publication. Citation information: DOI 10.1109/TPEL.2019.2912868, IEEE Transactions on Power Electronics

the BRLS adaptive filter (Fig.16(d)), it can be noted that the estimated position error obtained by the LMS adaptive filter (Fig.16(c)) can also be reduced to 4°. The estimated position error obtained by the LMS and BRLS adaptive filter in steady state is basically the same at different speed and load conditions.

D. Experimental Results of Disturbance Rejection

Fig.17 gives the estimated speed, the estimated position error and the estimated speed error during speed accelerating from 600 r/min to 1200 r/min, then decelerating to 600 r/min. Fig.17(a), (b), (c) show the experimental results with inverter nonlinearity compensation, with the LMS adaptive filter and with the BRLS adaptive filter, respectively. In Fig.17(a), it can be noted that the estimated position error is 8.2°and the estimated speed error is 10 r/min in steady state. They cannot be suppressed well by the inverter nonlinearity compensation. However in Fig.17(c) the estimated position error is 4.1°and the estimated speed error is 4.5 r/min in steady state. They can be significantly reduced by using the BRLS adaptive filter. In Fig.17(b), the estimated position and speed error are also reduced by using the LMS adaptive filter in steady state; but when the drive suddenly accelerates and decelerates, there exists larger estimated position /speed error than that given by the BRLS adaptive filter. The BRLS adaptive filter shows consistent performances at different operation conditions and is with the smallest transient estimated position and speed errors.

Fig.18 gives the estimated speed, the estimated position error and the estimated speed error under a step load change from 20% to 100% rated load at 900 r/min. Fig.18(a), (b), (c) give the experimental results with inverter nonlinearity compensation, with the LMS adaptive filter and with the BRLS adaptive filter, respectively. After enabling the BRLS adaptive filter, it can be observed that the estimated position error is reduced obviously with the load disturbance during the whole operation range. Compared with the inverter nonlinearity compensation method, the BRLS adaptive filter gives a better dynamic response with low harmonic ripples. The estimated position error arrives at 9.5°, 4.5° and the estimated speed error arrives at 9.5r/min, 5.4r/min in steady state, as shown respectively in Fig.18(a) and Fig.18(c). In Fig.18(b), the estimated position and speed errors are also suppressed in steady state by using the LMS adaptive filter. But compared with the method using the BRLS adaptive filter, it takes longer time to achieve the steady state with larger estimation error when suddenly loading and unloading the drive. So the proposed method by using the BRLS adaptive filter has good performance against load disturbances.

Fig.19 shows experimental results with load stepped from 0% to 20% rated load, then to 50% and 80% rated load, and finally to 100% rated load at 900 r/min when using the inverter nonlinearity compensation, using the LMS adaptive filter and using the proposed BRLS adaptive filter in Fig.19(a), (b), (c). In Table II, the *dq*-axes inductances obtained by finite element analysis at different load are given. From Table II, the L_q and L_d decrease with the increase of the load. Since the ada-

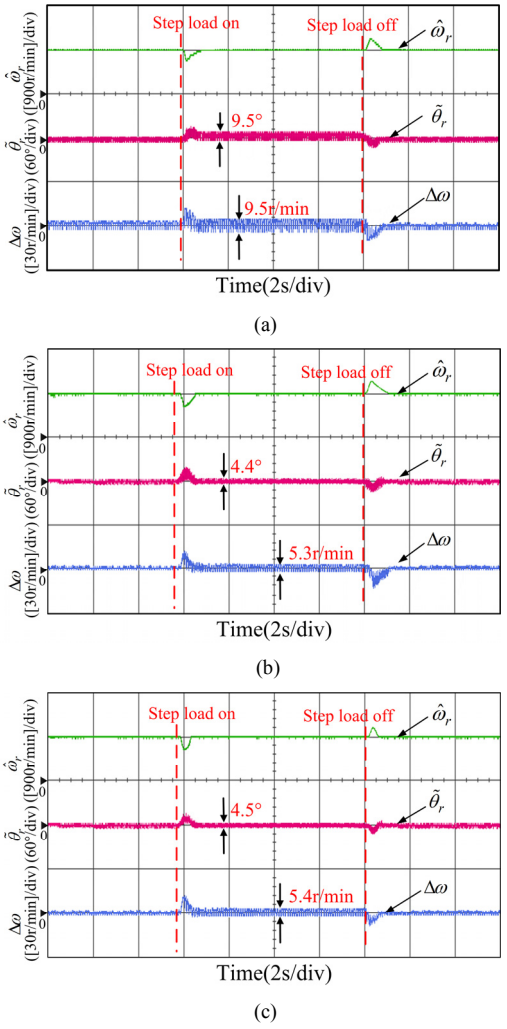

Fig. 18. Experimental results of the estimated speed error and the estimated position error with step load at 900 r/min. (a) With the inverter nonlinear voltage error compensation; (b) With the LMS adaptive filter; (c) With the BRLS adaptive filter.

-ptive filter is disabled, the harmonics in the *dq*-axes currents cannot be suppressed due to the existence of the 6th harmonic in the estimated position. The harmonic fluctuation is large in Fig.19(a). The estimated position error is within 9.3° and is still large with inverter nonlinear voltage error compensation only (Fig.19(a)). Observed from Fig.19(c), the *dq*-axes currents at different load conditions do not have noticeable 6th ripples. The estimated position error is within 5°at different load conditions. This illustrates that the proposed BRLS adaptive filter can adaptively estimate the 5th and 7th harmonics contained in the estimated back-EMF and then filter out them. So the 6th ripple in the position error is reduced. In Fig.19(b), the harmonic ripples in the *dq*-axes currents are also suppressed and the estimated position error is also within 4.9° at steady state by using the LMS adaptive filter. But there is a lager estimated position error when the load of IPMSM suddenly changes. So it can be concluded that

This article has been accepted for publication in a future issue of this journal, but has not been fully edited. Content may change prior to final publication. Citation information: DOI 10.1109/TPEL.2019.2912868, IEEE Transactions on Power Electronics

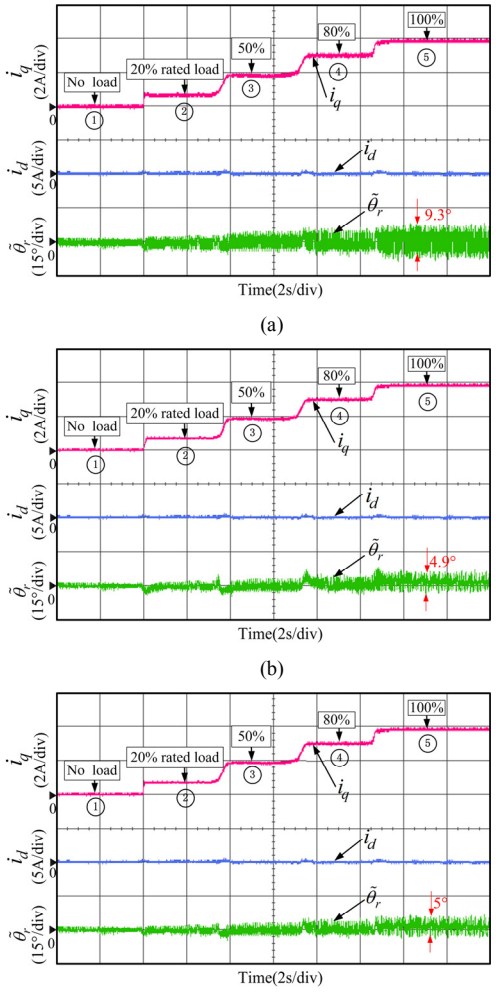

Fig. 19. Experimental results of dq-axes current and the estimated position error with respect to variation of load torque. (a) With the inverter nonlinearity voltage error compensation; (b) With the LMS adaptive filter; (c) With the BRLS adaptive filter.

TABLE II
DQ-AXES INDUCTANCES WITH DIFFERENT LOAD

		d-axis inductance/mH	*q*-axis inductance/mH
①	0% rated load	17.81	26.72
②	20% rated load	17.56	26.27
③	50% rated load	17.19	25.79
④	80% rated load	16.85	25.02
⑤	100% rated load	16.63	24.76

the proposed BRLS adaptive filter has also good performance against variations of the *dq*-axes inductances.

E. Experimental Results Compared to Resonant Filter

The resonant filter has now been widely used for harmonic suppression [38]-[39]. According to [38], it is noted that the resonant filter can filter out harmonic components completely when the system operates at a stable frequency. However, the resonant filter is sensitive to the variation of the frequency of signal to be processed. According to the bode diagram of the resonant filter given in Fig.20, a small frequency deviation would possibly result in a large phase shift. This could easily lead to a degradation of performance when it is applied in a variable speed drive. The resonant frequency of the resonant filter needs to be adaptively tuned by the estimated speed from the estimated back-EMF. In steady state, it may achieve good performance since harmonics in the back-EMF can be effectively suppressed by using the resonant filter. However the estimation error will be large during the dynamic transients of speed and load due to the difficulty in estimating the resonant frequency quickly and accurately during the transients. This will cause a failure of the sensorless drive. In order to observe this phenomenon clearly, the IPMSM drive is controlled with the position sensor and the estimated position and speed using the resonance filter during transients are recorded.

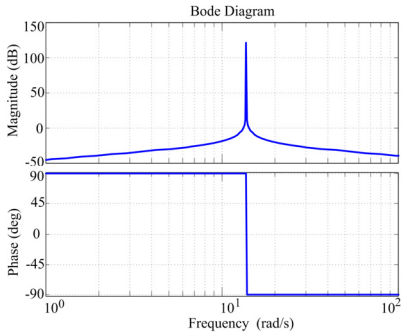

Fig. 20. Bode diagram of the resonant filter.

Fig.21 shows the experimental results of the rotor speed, the position and speed estimation errors respectively during the speed acceleration and deceleration with 50% rated load. Fig.21(a) gives the results using the resonant filter with the proposed method under sensorless control. The IPMSM accelerates from 600r/min to 1200r/min, and then decelerates to 600r/min. The corresponding maximum position and speed errors are 42°, 24r/min in Fig.21(a) while the maximum position and speed errors are 6.5°, 6 r/min only in Fig.21(b). In Fig.21(a), although the steady state error keeps relatively small, the estimation error will be significantly large in the acceleration and deceleration transients due to the difficulty in detecting the correct resonant frequency. On the contrary, the BRLS adaptive filter gives much better transient results as could be observed in Fig. 21(b).

Fig.22 shows experimental results at 900r/min with a step load disturbance from 20% to 100% rated load. Fig.22(a) gives the results using the resonant filter with the sensored control and the resonant frequency is tuned by the estimated speed while Fig.22(b) gives the results using the proposed BRLS adaptive filter under sensorless control. In Fig.22(a), the position estimation error keeps relatively small at steady state. The position estimation error increases during the large

This article has been accepted for publication in a future issue of this journal, but has not been fully edited. Content may change prior to final publication. Citation information: DOI 10.1109/TPEL.2019.2912868, IEEE Transactions on Power Electronics

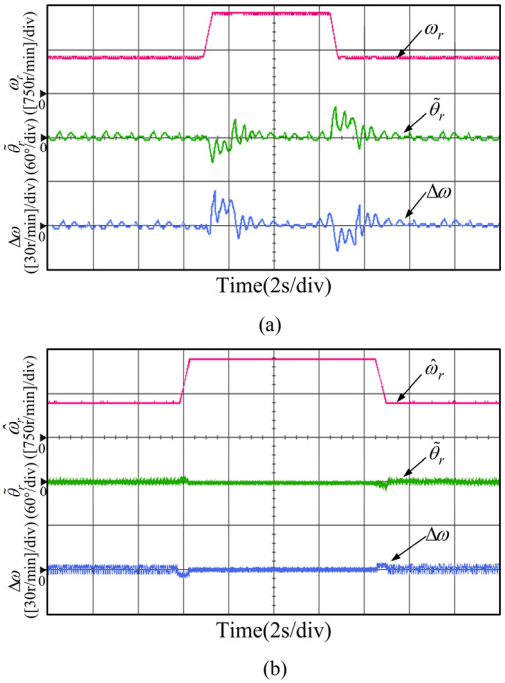

Fig. 21. Experimental results at speed acceleration and deceleration with 50% rated load; (a) with the resonant filter under sensored control; (b) with BRLS adaptive filter under sensorless control.

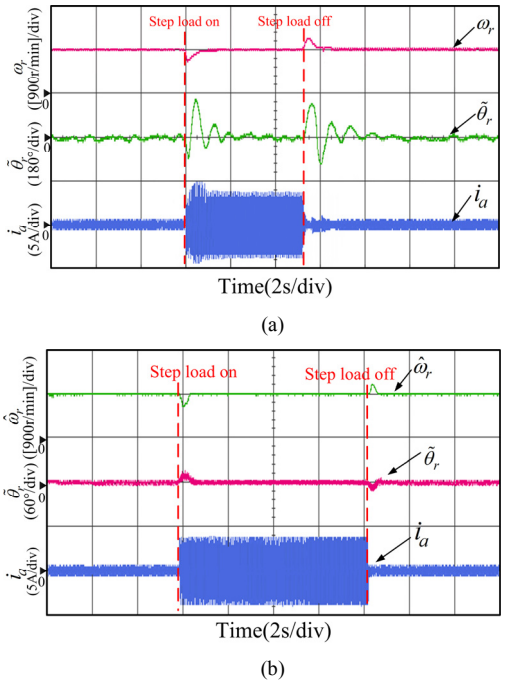

Fig. 22. Experimental results at 900r/min with step load disturbance. (a) with the resonant filter under sensored control; (b) with the BRLS adaptive filter under sensorless control.

load disturbance transient, and the maximum position error could reach as large as 160°. Thus the sensorless control for IPMSM will easily fail due to this large position estimation error. It is verified that a small frequency deviation would possibly result in a large phase shift as seen in Fig.20. From Fig.22(b), the proposed method with the BRLS adaptive filter can track the load change effectively and greatly reduce the harmonic ripples in the estimated position under sensorless control. Nevertheless, there is little difference between the dynamic and steady state performance in the proposed BRLS filter.

VI. Conclusion

In this paper, a back-EMF based sliding-mode observer combining the bilinear recursive least squares adaptive filter is proposed to filter out the harmonics contained in the estimated back-EMF, and hence to improve the estimated position accuracy of the sensorless IPMSM drive. The (6k±1)th harmonics in the estimated back-EMF and the (6k)th estimated position harmonic error caused by the inverter nonlinearity and flux linkage spatial harmonics are analyzed. With the BRLS adaptive filter, the inverter nonlinearity and machine spatial harmonics can be adaptively compensated at the same time. It can be observed from the experimental results that the BRLS adaptive filter can greatly suppress the fifth and seventh harmonic components in the estimated back-EMF. The sixth harmonic fluctuations contained in the estimated rotor position error are obviously reduced at different operating conditions. The robustness of the BRLS based sensorless control against machine parameter variation is also investigated. Through extensive comparative studies, it is evident that the proposed method using the BRLS adaptive filter can enhance the robustness and reduce the sensitivity of the sensorless drive to parameter variations and operation condition. The good performances of the BRLS filter sensorless drive and its high position estimation accuracy in different steady state dynamic operation conditions have been thoroughly verified.

References

[1] Z. Zhang, Y. Zhao, W. Qiao and L. Qu, "A Discrete-Time Direct Torque Control for Direct-Drive PMSG-Based Wind Energy Conversion Systems," *IEEE Trans. Ind. Appl.,* vol. 51, no. 4, pp. 3504-3514, Jul/Aug. 2015.

[2] M. Preindl and S. Bolognani, "Optimal State Reference Computation with Constrained MTPA Criterion for PM Motor Drives," *IEEE Trans. Power Electron.,* vol. 30, no. 8, pp. 4524-4535, Aug. 2015.

[3] X. Ge and Z.Q. Zhu, "Sensitivity of Manufacturing Tolerances on Cogging Torque in Interior Permanent Magnet Machines With Different Slot/Pole Number Combinations," *IEEE Trans. Ind. Appl.*, vol. 53, no. 4, pp. 3557-3567, Jul/Aug. 2017.

[4] G. Wang, D. Xiao, N. Zhao, X. Zhang, W. Wang and D. Xu, "Low-Frequency Pulse Voltage Injection Scheme Based Sensorless Control of IPMSM Drives for Audible Noise Reduction," *IEEE Trans. Ind. Electron.,* vol. 64, no. 11, pp. 8415-8426, Nov. 2017.

[5] G. Xie, K. Lu, S. K. Dwivedi, J. R. Rosholm and F. Blaabjerg, "Minimum-Voltage Vector Injection Method for Sensorless Control of PMSM for Low-Speed Operations," *IEEE Trans. Power Electron.,* vol. 31, no. 2, pp. 1785-1794, Feb. 2016.

[6] X. Zhou, B. Zhou, J. Yu, L. Yang and Y. Yang, "Research on Initial Rotor Position Estimation and Anti-Reverse Startup Methods for

DSEM," *IEEE Trans. Ind. Electron.,* vol. 64, no. 4, pp. 3297-3307, Apr. 2017.

[7] J. Holtz, "Acquisition of Position Error and Magnet Polarity for Sensorless Control of PM Synchronous Machines," *IEEE Trans. Ind. Appl.,* vol. 44, no. 4, pp. 1172-1180, Jul/Aug. 2008.

[8] J. Lara and A. Chandra, "Performance Investigation of Two Novel HSFSI Demodulation Algorithms for Encoderless FOC of PMSMs Intended for EV Propulsion," *IEEE Trans. Ind. Electron.,* vol. 65, no. 2, pp. 1074-1083, Feb. 2018.

[9] Q. Tang, A. Shen, X. Luo, J. Xu, "PMSM Sensorless Control by Injecting HF Pulsating Carrier Signal into ABC Frame," *IEEE Trans. Power Electron.,* vol. 32, no. 5, pp. 3767-3776, May. 2017.

[10] S. Murakami, T. Shiota, M. Ohto, K. Ide and M. Hisatsune, "Encoderless Servo Drive with adequately designed IPMSM for Pulse-Voltage-Injection-Based Position Detection," *IEEE Trans. Ind. Appl.,* vol. 48, no. 6, pp. 1922-1930, Nov./Dec. 2012.

[11] M. E. Haque, Limin Zhong , M. F. Rahman, "A Sensorless Initial Rotor Position Estimation Scheme for a Direct Torque Controlled Interior Permanent Magnet Synchronous Motor Drive," *IEEE Trans. Power Electron.*, vol.18, no. 6, pp.1376-1383, Nov. 2003.

[12] S. Yang, Y. Hsu, "Full Speed Region Sensorless Drive of Permanent-Magnet Machine Combining Saliency-Based and Back-EMF- Based Drive," *IEEE Trans. Ind. Electron.,* vol. 64, no. 2, pp. 1092-1101, Feb. 2017.

[13] Markus Seilmeier, Bernhard Piepenbreier, "Sensorless Control of PMSM for the Whole Speed Range Using Two- Degree-of-Freedom Current Control and HF Test Current Injection for Low-Speed Range," *IEEE Trans. Power Electron.,* vol. 30, no. 8, pp. 4394–4403, Aug. 2011.

[14] S. Kim, J. Im, E. Song, R. Kim, "A New Rotor Position Estimation Method of IPMSM Using All-Pass Filter on High-Frequency Rotating Voltage Signal Injection," *IEEE Trans. Ind. Electron.,* vol. 63, no. 10, pp. 5499-6509, Oct. 2016.

[15] C. Yu, J. Tamura, D. D. Reigosa , R. D. Lorenz, "Position self-sensing evaluation of a FI-IPMSM based on high-frequency signal injection methods," *IEEE Trans. Ind. Appl.*, vol. 49, no. 2, pp. 880-888, Mar/Apr. 2013.

[16] Y. Park, S. Sul, "Sensorless Control Method for PMSM Based on Frequency-Adaptive Disturbance Observer," *IEEE J. Emerg. Sel. Topics Power Electron.,* vol. 2, no. 2, pp. 143-151, Jun. 2014.

[17] G. Wang, J. Kuang, N. Zhao, G. Zhang, D. Xu, "Rotor Position Estimation of PMSM in Low-Speed Region and Standstill Using Zero-Voltage Vector Injection," *IEEE Trans. Power Electron.*, vol. 33, no. 9, pp. 7948-7958, Sep. 2018.

[18] X. Song, J. Fang, B. Han, S. Zheng, "Adaptive Compensation Method for High-Speed Surface PMSM Sensorless Drives of EMF-Based Position Estimation Error," *IEEE Trans. Power Electron.*, vol. 31, no. 2, pp. 1438-1449, Feb. 2016.

[19] Y. Zhao, Z. Zhang, W. Qiao, L. Wu, "An Extended Flux Model-Based Rotor Position Estimator for Sensorless Control of Salient-Pole Permanent-Magnet Synchronous Machines," *IEEE Trans. Power Electron*., vol. 30, no. 8, pp. 4412-4422, Aug. 2015.

[20] F. Genduso, R. Miceli, C. Rando , G. R. Galluzzo, "Back EMF Sensorless-Control Algorithm for High-Dynamic Performance PMSM," *IEEE Trans. Ind. Electron.*, vol. 57, no. 6, pp. 2092-2100, Jun. 2010.

[21] I. Boldea, M. C. Paicu, and G.D.Andreescu,"Active flux concept for motion-sensorless unified AC drives," *IEEE Trans. Power Electron*.,vol. 23, no. 5, pp. 2612–2618, Sep. 2008.

[22] S. A. Davari, D. A. Khaburi, F. Wang，R. M. Kennel,"Using full order and reduced order observers for robust sensorless predictive torque control of induction motors," *IEEE Trans. Power Electron*., vol. 27, no. 7, pp. 3424–3433, Jul. 2012.

[23] D. Liang, J. Li , R. Qu, "Sensorless Control of Permanent Magnet Synchronous Machine Based on Second-Order Sliding- Mode Observer With Online Resistance Estimation," *IEEE Trans. Ind. Appl.,* vol. 53, no. 4, pp. 3672-3682, Jul/Aug. 2017.

[24] Y. Fan, L. Zhang, M. Cheng , K. T. Chau, "Sensorless SVPWM-FADTC of a New Flux-Modulated Permanent-Magnet Wheel Motor Based on a Wide-Speed Sliding Mode Observer," *IEEE Trans. Ind. Electron*., vol. 62, no. 5, pp. 3143-3151, May. 2015.

[25] T. Bernardes, V. F.Montagner, H.A.Gründling, H.Pinheiro, "Discrete-Time Sliding Mode Observer for Sensorless Vector Control of Permanent Magnet Synchronous Machine," *IEEE Trans. Ind. Electron*., vol. 61, no. 4, pp. 1679-1691, Apr. 2014.

[26] Z. Qiao, T. Shi, Y. Wang, Y. Yan, C. Xia , X. He, "New Sliding-Mode Observer for Position Sensorless Control of Permanent-Magnet Synchronous Motor," *IEEE Trans. Ind. Electron*., vol. 60, no. 2, pp. 710-719, Feb. 2013.

[27] Y. Zhao, W. Qiao, L. Wu, "Dead-Time Effect Analysis and Compensation for a Sliding-Mode Position Observer-Based Sensorless IPMSM Control System," *IEEE Trans. Ind. Appl.*, vol. 51, no. 3, pp. 2528-2535, Jun. 2015.

[28] M.L.Corradini, G.Ippoliti, S.Longhi, and G.Orlando, "A quasi-sliding mode approach for robust control and speed estimation of PM synchronous motors," *IEEE Trans. Ind. Electron.*,vol. 59, no. 2, pp. 1096–1104, Feb. 2012.

[29] Y. Park, S. K. Sul, "A novel method utilizing trapezoidal voltage to compensate for inverter nonlinearity," *IEEE Trans. Power Electron.*, vol. 27, no. 12, pp. 4837–4846, Dec. 2012.

[30] Inoue Y, Yamada K, Morimoto S, et al, "Effectiveness of Voltage Error Compensation and Parameter Identification for Model-Based Sensorless Control of IPMSM," *IEEE Trans. Ind. Appl.*, vol. 45, no. 1, pp. 213-221, Jan/Feb. 2009.

[31] D. M. Park, K. H. Kim, "Parameter-Independent Online Compensation Scheme for Dead Time and Inverter Nonlinearity in IPMSM Drive Through Waveform Analysis," *IEEE Trans. Ind. Electron.*, vol. 61, no. 2, pp. 701-707, Feb. 2014.

[32] R. W. Hejny, R. D. Lorenz, "Evaluating the practical low-speed limits for back-EMF tracking-based sensorless speed control using drive stiffness as a key metric," *IEEE Trans. Ind. Appl.*, vol. 47, no. 3, pp. 1337–1343, May/Jun. 2011.

[33] S. Y. Kim, W. Lee, M. S. Rho, S. Y. Park, "Effective Dead-Time Compensation Using a Simple Vectorial Disturbance Estimator in PMSM Drives," *IEEE Trans. Ind. Electron.*, vol. 57, no. 5, pp. 1609-1614, May. 2010.

[34] Mikail Koc, JiabinWang, Tianfu Sun, "An Inverter Nonlinearity-Independent Flux Observer for Direct Torque-Controlled High-Performance Interior Permanent Magnet Brushless AC Drives," *IEEE Trans. Power Electron.,* vol. 32, no.1, pp. 490–502, Jan. 2017.

[35] P. Hutterer, H. Grabner, S. Silber, W. Amrhein, and W. Schaefer, "A study on systematic errors concerning rotor position estimation of PMSM based on back EMF voltage observation," *in Proc. IEEE Electr.Mach. Drives Conf.*, 2009, pp. 1393-1400.

[36] Jung S H, Kobayashi H, Doki S, et al,"An improvement of sensorless control performance by a mathematical modelling method of spatial harmonics for a SynRM," *in Proc. Power Electron. Conf.,* 2010, pp. 2010-2015.

[37] F. D. Freijedo, A. G. Yepes, J. Malvar, O. Lopez, P. Fernandez-Comesana, A. Vidal, J.Doval-Gandoy, "Frequency tracking of digital resonant filters for control of power converters connected to public distribution systems," *IET Power Electron.,* vol. 4,no. 4, pp. 454-462, Apr. 2011.

[38] Z. Q. Zhou, C. L. Xia, Y. Yan, Z. Q. Wang, and T.N.Shi, "Disturbances attenuation of permanent magnet synchronous motor d rives using cascaded predictive integral resonant controllers," *IEEE Trans. Power Electron.,* vol. 33, no. 2, pp. 1514-1527, Feb. 2018.

[39] C. Wu , H. Nian, "Stator harmonic currents suppression for DFIG based on feed-forward regulator under distorted grid voltage," *IEEE Trans. Power Electron.,* vol. 33 no. 2, pp. 1211-1224, Feb. 2017.

[40] Martin R, Kolossa D, "Techniques for Noise Robustness in Automatic Speech Recognition," *John Wiley & Sons.* 2012 pp. 51-85.

[41] R. Vullings, B. de Vries and J. W. M. Bergmans, "An Adaptive Kalman Filter for ECG Signal Enhancement," *IEEE Trans. Biome. Eng*., vol. 58, no. 4, pp. 1094-1103, Apr. 2011.

[42] Z. Szadkowski, D.Głas, "The Least Mean Squares Adaptive FIR Filter for Narrow-Band RFI Suppression in Radio Detection of Cosmic Rays," *IEEE Trans. Nucl. Sci*., vol. 64, no. 6, pp. 1304-1315, Jun. 2017.

[43] Choi. Y. S, Shin. H. C and Song. W. J, "Robust Regularization for Normalized LMS Algorithms," *IEEE Trans. Circuits Syst. II, Exp. Briefs*., vol. 53, no. 8, pp. 627-631, Aug. 2006.

[44] C. Elisei-Iliescu, C. Paleologu, R. A. Dobre, S. Ciochina and J. Benesty, "An RLS algorithm for the identification of bilinear forms," in *Proc. IEEE 23rd Int. Symp. Design Technol. Electron. Packag. (SIITME).*, 2017, pp. 292-295.

[45] Malakar, Bidhan, B. K. Roy, "A novel application of adaptive filtering for initial alignment of Strapdown Inertial Navigation System," *International Conference on Circuits, Systems, Communication and Information Technology Applications IEEE.*, 2014, pp. 189-194.
[46] Singh, Santosh Kumar, A. K. Goswami, N. Sinha, "Power system harmonic parameter estimation using Bilinear Recursive Least Square (BRLS) algorithm," *Int. J. Electr. Power Energy Syst*., vol. 67, PP. 1-10. May. 2015.
[47] Gin-Kou Ma, Junghsi Lee, V. J. Mathews, "A RLS bilinear filter for channel equalization," in *Proc. IEEE Int. Conf. Acoust., Speech, Signal Process*., 1994, pp. 257-260.
[48] Lee J, Mathews V J, "A stability result for RLS adaptive bilinear filters," *IEEE Signal Process. Lett.,* vol. 1, no. 12, pp. 191-193, Dec. 1994.
[49] Paulo S.R. Diniz, "Adaptive Filtering: Algorithms and Practical Implementation," New York, NY, USA: Springer, 2008, pp. 464-469.

Xuan Wu was born in Hunan, China, in 1983. He received the M.S. and Ph.D.degrees in Automation from the College of Electrical and Information Engineering, Hunan University, Changsha, China, in 2011 and 2016, respectively. He is a Associate researcher in the College of Electrical and Information Engineering, Hunan University. His research interests include permanent magnet synchronous motor drives, position sensorless control of AC motors.

Sheng Huang received the M.S. and Ph.D. degree both in College of Electrical and Information Engineering, Hunan University, Changsha, China, in 2012 and 2016, respectively. He is currently a Postdoc with the Center for Electric Power and Energy, Department of Electrical Engineering, Technical University of Denmark. His research interests include renewable energy generation, modeling and integration study of wind power, control of energy storage system, and voltage control.

Kan Liu (M'14-SM'17) received the B.Eng. and Ph.D. degrees in Automation from the Hunan University, China, in 2005 and 2011, respectively, and the Ph.D. degree in Electronic and Electrical Engineering from the University of Sheffield, Sheffield, U.K., in 2013. From 2013 to 2016, he was a research associate with the Department of Electronic and Electrical Engineering, the University of Sheffield. From 2016 to 2017, he was a lecturer with the Control Systems Group of the Loughborough University.
He is currently a Professor of Electro-mechanical Engineering at the Hunan University. His research interests include parameters estimation and sensorless control of permanent magnet synchronous machine drives and compensation of inverter nonlinearity, for applications ranging from automotive engineering to servo system. Prof. Liu serves as an Associate Editor for the IEEE Access, and also a Guest Editor/Associate Editor for the Journal of Control Science and Engineering, the International Journal of Rotating Machinery, and the CES Transactions on Electrical Machines and Systems. He is also the Acting Director of the Engineering Research Center of the Ministry of Education on Automotive Electronics and Control Technology.

Kaiyuan Lu (M'11) received the B.S. and M.S. degrees from Zhejiang University, Zhejiang, China, in 1997 and 2000 respectively, and the Ph.D. degree from Aalborg University, Denmark, in 2005, all in electrical engineering. In 2005, he became an Assistance Professor with the Department of Energy Technology, Aalborg University, where he has been an Associate Professor since 2008. His research interests include design of permanent magnet machines, finite element method analysis, and control of permanent magnet machines.

Yashan Hu received the B.Eng. and M.Sc. Degrees from the Northwestern Polytechnical University, Xi'an, China, in 2002 and 2005, respectively and the Ph.D. degree from the University of Sheffield, Sheffield, U.K, in 2016, all in Electronic and Electrical Engineering. From 2016 to 2018, he was with Siemens Wind Power A/S (Denmark) as an advanced research engineer. Since 2018, he has been an Associate Professor in the College of Electrical and Information Engineering at Hunan University. His current research interests include power electronic systems and control, and wind energy conversion systems.

Wenli Pan received the B.S. degree in electrical engineering and automation from Northeast Normal University, Changchun, China, in 2016. She is currently working toward the M.S. degree in control science and engineering in the College of Electrical and Information Engineering, Hunan University. Her current research interests include permanent magnet synchronous motor drive and position sensorless control.

Xiaoyan Peng received the B.S. and M.S. degrees in mechanical engineering, and the Ph.D. degree in automatic control from Hunan University, Changsha, China, in 1986, 1989, and 2013, respectively. She is currently a Professor with the College of Mechanical and Vehicle Engineering, Hunan University, Changsha, China. Her research interests include control of mechatronic systems and safety analysis of autonomous vehicles.